Stochastic Geometry-Based Analysis of Cell-Free Massive MIMO Systems With Aerial Users

Yujie Qin, *Member, IEEE*, Mustafa A. Kishk, *Member, IEEE*, and Mohamed-Slim Alouini, *Fellow, IEEE*

***Abstract*— Cell-free massive multiple-input-multiple-output (CF-mMIMO) systems are promising deployment paradigms for next-generation networks. They comprise a large number of base stations (BSs) and simultaneously serve all users over the same time and frequency resources. We analyze the performance of integrating aerial users, such as unmanned aerial vehicles (UAVs), into this novel system. Specifically, we consider a CF-mMIMO network containing both ground and aerial users and study the influence of system parameters on the signal-to-interference-plus-noise ratio (SINR) and rate coverage performance. Additionally, we use tools from stochastic geometry to capture the spatial randomness of users and BSs and compare the performance of the CF-mMIMO system to that of traditional small cell systems. Given the improvement of dedicated antennas, such as up-tilted/down-tilted antennas, on the performance of small cell systems, we include the up-tilted/down-tilted antenna model in this work and analyze the omnidirectional antenna model as a special case. We derive both the exact expressions and dominant-signal-based approximations for SINR and rate coverage. Our numerical results demonstrate that the CF-mMIMO system exhibits better performance at low values of SINR and rate thresholds and higher minimum achievable SINR compared to the small cell system. Furthermore, we observe that users benefit dramatically from increasing altitudes and establishing line-of-sight (LoS) channels with BSs.**

***Index Terms*— Cell-free massive MIMO, aerial users, stochastic geometry, small cell, coverage probability, achievable rate.**

I. Introduction

UNMANNED aerial vehicles (UAVs), also referred to as drones, have shown great potential and a wide range of applications in next-generation communications and transportation. Given their high flexibility and mobility, UAVs are able to deliver packages [1] and act as aerial base stations to track and serve users in real-time based on demand [2], [3], [4], [5], provide cellular coverage to remote areas [6], [7], conduct surveillance, and even perform multiple tasks simultaneously [8], [9]. Consequently, integrating UAVs into current wireless communication networks and establishing reliable connectivity between UAVs and base stations have become hot research topics.

Meanwhile, cooperative cellular networks have been the subject of much investigation throughout the past decade, in which a set of BSs equipped with single or multiple antennas simultaneously serve a set of users. Typically, cell-free massive multiple-in-multiple-out (CF-mMIMO) architecture is viewed as a key solution to the increasing demand of data rate as it combines the best aspects of mMIMO and ultra-dense networks [10], e.g., take advantages of the accompanying high spectral and energy efficiency and simple signal processing, and avoids the inter-cell interference and large quality-of-service (QoS) variations. In CF-mMIMO networks, a large number of BSs with single or multiple antennas are deployed to serve a smaller number of users in the same time and frequency resources, and these BSs are connected via a backhaul network to a central processing unit (CPU) to process the data [11]. At the same time, [12] shows that CF-mMIMO outperforms small cell systems in terms of 95%-likely per-user throughput and provides uniformly good performance to all users, and [10] shows that its low-complexity user-centric alternative also provides good performance to users.

Noticing the potential widespread deployment of CF-mMIMO in future wireless communication networks, it becomes crucial to analyze the performance of aerial users, such as UAVs (in this study, we select UAVs due to their previously mentioned potential). Therefore, motivated by the diverse applications of UAVs and the promising performance of CF-mMIMO architecture, we investigate the performance of UAV users within CF-mMIMO systems. We analyze the impact of various system parameters, including altitudes, fading parameters, and BS densities, on network performance. Additionally, building upon our previous work demonstrating the capability of dedicated aerial base stations to enhance the signal-to-interference-plus-noise ratio (SINR) coverage probability of aerial users [13], we examine the performance of CF-mMIMO systems using the same antenna model, namely up-tilted/down-tilted antennas.

A. Related Works

Literature related to this work can be categorized into: (i) existing methods of improving the Quality of Service (QoS) of aerial users, (ii) CF-mMIMO-related analysis, and (iii) stochastic geometry-based analysis of CF-mMIMO

Received 4 December 2023; revised 13 June 2024 and 26 September 2024; accepted 22 November 2024. Date of publication 5 December 2024; date of current version 17 July 2035. This work was supported by KAUST Office of Sponsored Research. The associate editor coordinating the review of this article and approving it for publication was J. Liu. *(Corresponding author: Mustafa A. Kishk.)*

Yujie Qin and Mohamed-Slim Alouini are with the Computer, Electrical and Mathematical Sciences and Engineering (CEMSE) Division, King Abdullah University of Science and Technology (KAUST), Thuwal 23955, Saudi Arabia (e-mail: yujie.qin@kaust.edu.sa; slim.alouini@kaust.edu.sa).

Mustafa A. Kishk is with the Department of Electronic Engineering, Maynooth University, Maynooth, W23 F2H6 Ireland (e-mail: mustafa.kishk@mu.ie).

Digital Object Identifier 10.1109/TCOMM.2024.3511948

0090-6778 © 2024 IEEE. All rights reserved, including rights for text and data mining, and training of artificial intelligence and similar technologies. Personal use is permitted, but republication/redistribution requires IEEE permission.
See https://www.ieee.org/publications/rights/index.html for more information.
Authorized licensed use limited to: Maynooth University Library. Downloaded on September 23,2025 at 15:50:34 UTC from IEEE Xplore. Restrictions apply.

systems. A brief discussion of related works in each of these categories follows.

1) Existing Methods of Improving the QoS of Aerial Users: Given the unprecedented advances in aerial transportation in recent years, the QoS of aerial communication has garnered significant attention [14], [15]. Aerial dedicated BSs were proposed in [13], where the authors considered adjusting a fraction of down-tilted BSs into up-tilted BSs to serve aerial users. Additionally, in [16], the authors studied Max-Min SINR UAV trajectory design based on aerial dedicated BSs. In [17], the downlink inter-cell interference coordination mechanism was applied to aerial command and traffic control to enhance the reliability of aerial connectivity. Furthermore, [18], [19] extended models for ground-to-ground (G2G) links to air-to-ground (A2G) channels and analyzed altitude-dependent path-loss exponents and fading functions. Aerial user trajectory optimization was explored in [20] and [21] to improve network energy efficiency. In [22], massive MIMO systems were utilized to enhance connectivity between UAVs and ground BSs. Additionally, a study in [23] investigated a deep reinforcement learning-based intelligent navigation task for cellular-connected UAV networks, aiming to minimize the weighted sum of time cost and expected outage duration alongside UAV trajectory. Furthermore, [24] analyzed uplink precoding optimization for NOMA cellular-connected UAV networks. A 5G New Radio-based analysis for vehicle-to-everything (V2X) communication was presented in [25] and [26], where the authors proposed a resource allocation scheme to reduce resource collisions and achieve improved performance and ubiquitous service. In [27], the authors employed a digital twin-based distillation method to enhance the operational accuracy of aerial users. A multi-UAV cooperation system with resource allocation was analyzed in [28] to optimize UAV resource utilization and reduce processing delay. Additionally, deep learning and graph theory were jointly employed in [29] to reduce the transmission delay of aerial users.

2) CF-mMIMO-Related Analysis: Authors in [30] provided a comprehensive survey on CF-mMIMO, which discussed the system model, system operations, practical perspectives, and future research directions of CF-mMIMO systems, and the authors in [31] provided a overview about using CF-mMIMO in 6G networks and talked out the open questions. CF-mMIMO systems with channel estimation errors, power control, non-orthogonal pilot sequences, and correlated and uncorrelated channels were investigated in [12] and [32], where the authors showed that CF-mMIMO systems can significantly outperform small cell systems in terms of throughput. Authors in [33] provided a discussion on CF-mMIMO from the perspective of energy efficiency and quantified a range of open issues. A scalable CF-mMIMO system was analyzed in [34], [35] by exploiting the dynamic cooperation cluster concept from the Network MIMO literature. The performance of a CF-mMIMO system with multi-antenna access points (APs) and full-pilot zero-forcing precoding was analyzed in [36], while local partial zero-forcing precoding was analyzed in [37]. A deep learning-based power allocation approach in CF-mMIMO systems was analyzed in [38], and hardware impairments-related analysis was provided in [39], [40], [41]. Regarding aerial users, authors in [11], [42] studied the performance of a CF-mMIMO network containing both aerial and ground users, with [11] focusing more on power allocation and [42] on the user-centric approach. The authors in [43] analyzed the integration of reconfigurable intelligent surfaces into CF-mMIMO systems and derived closed-form expressions for the lower-bound achievable spectral efficiency.

3) Stochastic Geometry-Based Analysis of CF-mMIMO Systems: Stochastic geometry-based analysis of the performance of CF-mMIMO networks was initially explored in [44], where the authors analyzed coverage probability based on the Poisson point process (PPP) distributed BSs. In contrast to [44], which primarily focused on performance metrics, authors in [45] utilized stochastic geometry to analyze CF-mMIMO systems, emphasizing phenomena such as channel hardening and favorable propagation. From the perspective of fronthaul capacity, [46] investigated the rate coverage performance of CF-mMIMO systems with finite fronthaul capacity, adopting a user-centric approach where the locations of users and BSs are modeled by independent PPPs, and users are served only by the nearest several BSs. A study on simultaneous wireless information and power transfer (SWIPT)-based performance analysis of CF-mMIMO users was conducted in [47], considering both linear and non-linear energy harvesting models. To address the Doppler shift effect on CF-mMIMO system performance, [48] explored frame length selection techniques to mitigate the effect and provided lower bounds on average downlink and uplink rates using stochastic geometry tools. Additionally, [49] investigated the uplink performance of CF-mMIMO systems supported by mmWave. Security performance analysis of CF-mMIMO systems was presented in [50], where the locations of access points (APs), users, and eavesdroppers are modeled by three independent PPPs. Furthermore, for edge computing scenarios, [51] offered insights into the energy-efficient design of edge computing-enabled CF-mMIMO systems.

B. Contributions

This work investigates the performance of CF-mMIMO systems which are mixed of ground and aerial users and compares its performance with small cell systems. Different from related works, we use tools from stochastic geometry to model the spatial randomness of users and BSs, and use the Nakagami-m model to capture the multi-path fading. The main contributions are summarized as follows.

- We consider a CF-mMIMO system mixed with ground and aerial users and model the locations of BSs and users by independent PPP and binomial point process (BPP). We model the communication channels by Nakagami-m fading models and use the minimum mean square error technique to estimate the channels. Besides, we consider the up-tilted/down-tilted antenna model and analyze the omnidirectional antenna model as a special case.
- We derive the SINR and rate coverage expressions for the CF-mMIMO systems and propose an approximation that

Authorized licensed use limited to: Maynooth University Library. Downloaded on September 23,2025 at 15:50:34 UTC from IEEE Xplore. Restrictions apply.

TABLE I
NOTATION TABLE

Notations	Description
Φ_b, λ_b	Poisson point process of BSs and its density
$\Phi_{b,ub}$, $\Phi_{b,db}$, δ	Locations of up-tilted and down-tilted BSs, and their densities
$S(\mathcal{A})$	Space of an area $\mathcal{A}$
N_{bs}, N_a, M,	Number of BSs, antennas per BS, total antennas
$\mathcal{N}(\mathbf{au})$, $\mathcal{N}(\mathbf{gu})$, K,	Number of aerial users, ground users, total users
Δh_{au}, Δh_{gu}	Altitudes of aerial users, and ground users
r_{wk}	Euclidean distance between the w-th BS and the k-th user
l_{wk}	non-singular bounded path-loss model
$\mathbf{g}_{wk}$	Channel vector between the w-th BS and the k-th user
$\mathbf{h}_{wk}$	Small-scale fading between the w-th BS and the k-th user
$P_l(r)$, $P_n(r)$	LoS and NLoS probability given Euclidean distance r
$\mathbf{au}$, $\mathbf{au}$	Locations of aerial users, and ground users
$\mathcal{G}_{\{\cdot\},ub}(z)$, $\mathcal{G}_{\{\cdot\},ub}(z)$	Antenna gains of up-tilted antenna, and down-tilted antenna
$\mathbf{y}_w$	Received signal of the w-th BS
$\boldsymbol{\psi}_i$	The i-th orthogonal pilot sequence
τ_{tr}, τ_c	Length of pilot sequence, and channel coherence length
ρ_p, ρ_d	Uplink and downlink pilot SNR
$\mathbf{n}_{tr}$, n_o	Noise vector uplink, and downlink transmission
$\mathbf{x}_w$	Transmit signal of the w-th BS
η_{wi}	Power coefficient of the w-th BS to the i-th user
s_i	Data signal to the i-th user
θ,γ	SINR threshold, rate coverage threshold
$P_{\text{cov}}(\theta)$, Ra^{cf}	Coverage probability, rate coverage (CF-mMIMO)
$P_{\text{cov}}^{\text{sc}}(\theta)$, Ra^{sc}	Coverage probability, rate coverage (small cell)

is based on computing the dominant signal (not necessarily the nearest BS due to antenna gain) exactly and the remaining signal in average. The proposed approximation highly reduces the computation complexity and provides a tight result to the simulation.

- We study several system parameters, such as aerial user altitudes, environment parameters, Nakagami-m fading parameters, and BS densities, on the performance of CF-mMIMO systems and compare the performance to the small cell systems.
- To the best of our knowledge, our work is the first to use stochastic geometry tools to evaluate the CF-mMIMO systems containing both ground and aerial users. Our numerical results reveal that CF-mMIMO systems outperform small cell systems at minimum achievable SINR and data rates, and CF-mMIMO systems benefit greatly from increasing the user altitudes.

II. SYSTEM MODEL

We consider a CF-mMIMO system containing BSs, aerial users, and ground users. In particular, we consider two types of BSs: up-tilted BSs and down-tilted BSs. The up-tilted BSs are dedicated to serving aerial users by up-tilting their beams, while the down-tilted BSs are traditional ground BSs, as shown in Fig. 1. Additionally, the notations used in this work are summarized in Table I.

We consider a finite space $\mathcal{A}$, which is a circle with radius r_s, with area $S(\mathcal{A}) = \pi r_s^2$ m^2, and the locations of BSs are modeled by a PPP Φ_b with density λ_b, in which a fraction δ of BSs are up-tilted BSs. The locations of users, aerial and ground users, are modeled by a binomial point process (BPP). Therefore, the density of up-tilted BSs is $\lambda_{b,ub} = \delta\lambda_b$ and the density of down-tilted BSs is $\lambda_{b,db} = (1-\delta)\lambda_b$, and the locations of up-tilted BSs $\Phi_{b,ub}$ and the locations of down-tilted BSs $\Phi_{b,db}$ are two independent PPPs which can be obtained by independent thinning of Φ_b. Consequently, the number of BSs is a Poisson random variable with mean

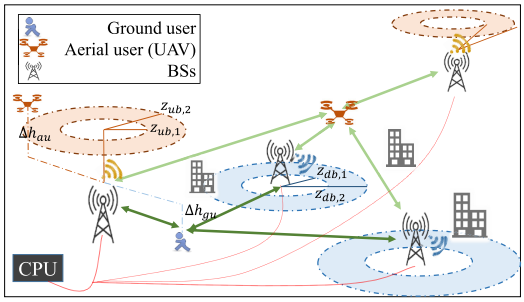

Fig. 1. Illustration of system model. The system is composed of aerial users, ground users, up-tilted BSs and down-tilted BSs.

$\mathbb{E}[N_{bs}] = \lambda_b S(\mathcal{A})$. Assume that each BS has N_a antennas, $N_a \geq 1$, hence, the total number of antennas existing in $\mathcal{A}$ is $M = N_a N_{bs}$. We consider that each user is equipped with a single antenna and let $K = \mathcal{N}(\mathbf{au})+\mathcal{N}(\mathbf{gu})$ be the summation of the number of single antenna UAV users, $\mathbf{au}$, and ground users, $\mathbf{gu}$, which satisfy $K \ll M$ [12], [46], $\mathbf{au}$ and $\mathbf{gu}$ are the locations of UAV users and ground users.

In the CF-mMIMO system, all N_{bs} BSs simultaneously serve all K users, and the downlink transmission and uplink transmission proceed by time-division duplex (TDD) operation. That is, each coherence interval includes an uplink training phase, a downlink payload, and an uplink payload transmission phase. Without loss of generality, we focus on the typical user located at the origin, with a probability of $\frac{\mathcal{N}(\mathbf{au})}{K}$ to be an aerial user and a probability of $\frac{\mathcal{N}(\mathbf{gu})}{K}$ to be a ground user, to conduct the analysis and investigate the system performance.

In what follows, we introduce the channel models, antenna models, and uplink training phase.

A. Channel Model

We consider that the channels between the user and antennas from different BSs undergo different large-scale fading while the antennas from the same BS go through the same large-scale fading but i.i.d. small-scale fading. That is, let $\mathbf{g}_{wk} \in \mathbb{C}^{N_a \times 1}$ be the channel vector between the w-th BS and the k-th user, the communication link can either be line-of-sight (LoS), denoted by $\mathbb{1}(\text{LoS})$, or non-LoS (NLoS), denoted by $\mathbb{1}(\text{NLoS})$,

$$\mathbf{g}_{wk} = \mathbb{1}(\text{LoS}) l_{wk,l}^{1/2} \mathbf{h}_{wk,l} + \mathbb{1}(\text{NLoS}) l_{wk,n}^{1/2} \mathbf{h}_{wk,n}, \quad (1)$$

in which $l_{wk,c} = \max(1, r_{wk}^{-\alpha_c})$ is the non-singular bounded path-loss model and $r_{\{\cdot\}}$ is the Euclidean distance between the BS and the user, where the subscript $c \in \{l, n\}$ depends on the LoS or NLoS link, and r_{wk} is the distance between the w-th BS and k-th user. $\mathbf{h}_{wk,c} \in \mathbb{C}^{N_a \times 1}$ contains the small-scale fading elements, which are i.i.d. random variables with each $i \in \{1, \cdots, N_a\}$ has $|h_{wk}(i)|$ following a Nakagami-m probability density function (PDF) and $|h_{wk}(i)|^2$ following a Gamma distribution

$$f_{|h_{wk}(i)|^2}(x) = \frac{m_c^{m_c} x^{m_c-1}}{\Gamma(m_c)} \exp(-m_c x), \quad (2)$$

in which $\Gamma(x)$ is a gamma function and m_c denotes the shape parameter, $m_c = \{m_l, m_n\}$ in the case of LoS and

Authorized licensed use limited to: Maynooth University Library. Downloaded on September 23,2025 at 15:50:34 UTC from IEEE Xplore. Restrictions apply.

NLoS transmission, respectively. Besides, we have $\mathbb{E}[\mathbf{h}_{wk,l}] = \mathbb{E}[\mathbf{h}_{wk,n}] = \mathbf{0}_{N_a\times 1}$, $\mathbb{E}[|\mathbf{h}_{wk,l}|^2] = \mathbb{E}[|\mathbf{h}_{wk,n}|^2] = \mathbf{1}_{N_a\times 1}$ and $\mathbb{E}[|\mathbf{h}_{wk,l}|^4] = (\mathbf{1}+\mathbf{1}/\mathbf{m_l})_{N_a\times 1}$, $\mathbb{E}[|\mathbf{h}_{wk,n}|^4] = \mathbf{2}_{N_a\times 1}$. The probability of establishing LoS communication channel depends on the Euclidean distance and the altitude difference, given in [52] as

$$P_l(r) = \frac{1}{1+e_1\exp(-e_2(\frac{180}{\pi}\arctan(\frac{\Delta h_{\{au,gu\}}}{r})-e_1))}, \tag{3}$$

where e_1 and e_2 are two environment variables and $\Delta h_{\{au,gu\}}$ is the height difference between aerial users, ground users and BSs, respectively. Consequently, the probability of NLoS link is $P_n(r) = 1 - P_l(r)$.

B. Antenna Models

We use the same antenna model as our previous work [13]. Users in the network either experience main lobe or sidelobe gain from an up-tilted/down-tilted BS, which depends on the positions. Let $v \in \{\mathbf{gu}, \mathbf{au}\}$ be a general user. While the up-tilted BSs are dedicated to aerial users, all ground users experience sidelobe from up-tilted BSs. Similar to down-tilted BSs and aerial users. The antenna gain provided by an up-tilted/down-tilted BS with horizontal distance z to v is given by

$$\mathcal{G}_{v,ub}(z) = \begin{cases} \zeta_m & , \quad z_{ub,1} < z < z_{ub,2}, v \in \{\mathbf{au}\}, \\ \zeta_s & , \quad \text{otherwise}, \end{cases}$$
$$\mathcal{G}_{v,db}(z) = \begin{cases} \zeta_m & , \quad z_{db,1} < z < z_{db,2}, v \in \{\mathbf{gu}\}, \\ \zeta_s & , \quad \text{otherwise}, \end{cases} \tag{4}$$

in which the subscript $\{ub, db\}$ denotes the up-tilted and down-tilted BSs, respectively, and $z_{ub,1} = \Delta h_{au}\cot(\theta_{ub} + \frac{\phi_{ub}}{2})$, $z_{ub,2} = \Delta h_{au}\cot(\theta_{ub} - \frac{\phi_{ub}}{2})$, $z_{db,1} = \Delta h_{gu}\cot(\theta_{db} + \frac{\phi_{db}}{2})$, $z_{db,2} = \Delta h_{gu}\cot(\theta_{db} - \frac{\phi_{db}}{2})$, where θ_{ub} and θ_{db} are the up-tilt and down-tilt angle of the BS antenna, respectively, and ϕ_{ub} and ϕ_{db} are the vertical antenna beamwidth of the up-tilted BSs and down-tilted BSs, respectively.

C. Uplink Channel Estimation

In the uplink training phase, all K users simultaneously send orthogonal pilot sequences, $\boldsymbol{\psi}_i \in \mathbb{C}^{\tau_{tr}\times 1}$, with duration equal to $\tau_{tr} < \tau_c$, where τ_c is the dimension in time/frequency samples of the channel coherence length. Let z_{wi} be the Euclidean distance between the BS w and the user i, therefore, the signal received by the w-th BS during the training phase is $\mathbf{y}_w \in \mathbb{C}^{N_a\times\tau_{tr}}$,

$$\begin{aligned}\mathbf{y}_w &= \sum_{i=1}^{\mathcal{N}(\mathbf{au})}\sqrt{\tau_{tr}\rho_p}\mathcal{G}_{au,b}(z_{w_b i})\mathbf{g}_{w_b i}\boldsymbol{\psi}_i^H \\ &\quad + \sum_{j=1}^{\mathcal{N}(\mathbf{gu})}\sqrt{\tau_{tr}\rho_p}\mathcal{G}_{gu,b}(z_{w_b j})\mathbf{g}_{w_b j}\boldsymbol{\psi}_j^H + \mathbf{n}_{tr} \\ &= \sum_{l=1}^{K}\sqrt{\tau_{tr}\rho_p}\mathcal{G}_{v,b}(z_{wk})\mathbf{g}_{wl}\boldsymbol{\psi}_l^H + \mathbf{n}_{tr}, \end{aligned} \tag{5}$$

where the superscript H denotes the conjugate transpose, $b \in \{ub, db\}$ denotes the up-tilted BSs or down-tilted BSs (which depends on which type of tilt is the n-th BS), ρ_p denotes the uplink pilots' signal-to-noise ratio (SNR), $\boldsymbol{\psi}_{\{i,j\}} \in \mathbb{C}^{\tau_{tr}\times 1}$ is the pilot sequence sent by user $\{i, j\}$, $\boldsymbol{\psi}_i^H\boldsymbol{\psi}_j = \delta_{ij}$, and $\mathbf{n}_{tr}$ denotes the additive noise vector at the BS which is a $N_a \times \tau_{tr}$ matrix with elements i.i.d. $\mathcal{CN}(0,1)$.

The w-th up-tilted BS estimates the channel of the k-th user by projecting $\mathbf{y}_w$ onto $\frac{1}{\sqrt{\rho_p\tau_{tr}}}\boldsymbol{\psi}_k$,

$$\begin{aligned}\mathbf{y}_{wk} &= \frac{1}{\sqrt{\rho_p\tau_{tr}}}\mathbf{y}_w\boldsymbol{\psi}_k = \sum_{i=1}^{K}\mathcal{G}_{v,b}(z_{wi})\mathbf{g}_{wi}\boldsymbol{\psi}_i^H\boldsymbol{\psi}_k \\ &\quad + \frac{1}{\sqrt{\rho_p\tau_{tr}}}\mathbf{n}_{tr}\boldsymbol{\psi}_k, \end{aligned} \tag{6}$$

where the term $\sum_{i\neq k}\boldsymbol{\psi}_i^H\boldsymbol{\psi}_k$ is due to the pilot contamination.

Assuming the distance-dependent pathloss l_{wk} is known a priori, and the BS estimates the channel by using minimum-mean-squared-error estimation. Let $\hat{\mathbf{g}}_{wk}$ be the estimated channel vector at w-th BS and $\tilde{\mathbf{g}}_{wk}$ is the channel estimation error,

$$\begin{aligned}\hat{\mathbf{g}}_{wk} &= \mathbb{E}[\mathbf{g}_{wk}\mathbf{y}_{wk}^H](\mathbb{E}[\mathbf{y}_{wk}\mathbf{y}_{wk}^H])^{-1}\mathbf{y}_{wk}, \\ \tilde{\mathbf{g}}_{wk} &= \mathbf{g}_{wk} - \hat{\mathbf{g}}_{wk}. \end{aligned} \tag{7}$$

D. Conjugate Beamforming

In this work, we consider that BSs use conjugate beamforming technology to serve K users. With conjugate beamforming precoding, the n-th BS transmits the signal

$$\mathbf{x}_w = \sqrt{\rho_b}\sum_{i=1}^{K}\sqrt{\eta_{wi}}\hat{\mathbf{g}}_{wi}^* s_i, \tag{8}$$

in which $()^*$ denotes the conjugate, ρ_b is the transmit power limit of each BS, η_{wi} is the power coefficient of the w-th BS for the transmission to the i-th user, and s_i is the data signal to the i-th user, in which $\mathbb{E}[|s_i|^2] = 1$. Consequently, the downlink received signal of the typical user is

$$\begin{aligned} p_{r,o} &= \sum_{w=1}^{N_{bs}}\mathcal{G}_{o,b}(z_{wo})\mathbf{g}_{wo}^T\mathbf{x}_w + n_o \\ &= \sum_{w=1}^{N_{bs}}\sum_{i=1}^{K}\sqrt{\rho_b\eta_{wi}}\mathcal{G}_{o,b}(z_{wo})\mathbf{g}_{wo}^T\hat{\mathbf{g}}_{wi}^* s_i + n_o \\ &= \sum_{w=1}^{N_{bs}}\sqrt{\rho_b\eta_{wo}}\mathcal{G}_{o,b}(z_{wo})\mathbb{E}[\hat{\mathbf{g}}_{wo}^T\hat{\mathbf{g}}_{wo}^*]s_o \\ &\quad + \sum_{w=1}^{N_{bs}}\sqrt{\rho_b\eta_{wi}}\mathcal{G}_{o,b}(z_{wo})(\hat{\mathbf{g}}_{wo}^T\hat{\mathbf{g}}_{wo}^* - \mathbb{E}[\hat{\mathbf{g}}_{wo}^T\hat{\mathbf{g}}_{wo}^*])s_o \\ &\quad + \sum_{w_b=1}^{N_{bs}}\sum_{i\neq o}^{K}\sqrt{\rho_b\eta_{wi}}\mathcal{G}_{o,b}(z_{wo})\hat{\mathbf{g}}_{wo}^T\hat{\mathbf{g}}_{wi}^* s_i \\ &\quad + \sum_{w=1}^{N_{bs}}\sum_{i=1}^{K}\sqrt{\rho_b\eta_{wi}}\mathcal{G}_{o,b}(z_{wo})\tilde{\mathbf{g}}_{wo}^T\hat{\mathbf{g}}_{wi}^* s_i + n_o, \end{aligned} \tag{9}$$

where the subscript o denotes the typical user, $o \in \{\mathbf{au}, \mathbf{gu}\}$ and n_o denotes the noise in downlink transmission,

Authorized licensed use limited to: Maynooth University Library. Downloaded on September 23,2025 at 15:50:34 UTC from IEEE Xplore. Restrictions apply.

$n_o \sim \mathcal{CN}(0,1)$. Besides, the first term in (9) is the desired signal, the second term is due to the beamforming uncertainty, the third term denotes the inter-user interference, and the forth term is caused by channel estimation error.

The SINR at the typical user is obtained by the ratio of the power of the desired signal and the power of the remaining terms in (9). Here, the signal and interference are obtained by the mean due to the uplink channel estimation [11], [12], [44], [46].

Definition 1 (SINR of the CF-mMIMO user): The SINR of a CF-mMIMO user is given by

$$\mathrm{SINR} = \frac{\mathbb{E}[|T_0|^2]}{1+\mathbb{E}[|T_1|^2]+\mathbb{E}[|T_2|^2]+\mathbb{E}[|T_3|^2]}, \tag{10}$$

in which $|T_0|$ denotes the desired signal, $|T_1|$ is the beamforming gain uncertainty, $|T_2|$ denotes the interference from other users, and $|T_3|$ is channel estimation error,

$$\begin{aligned}
\mathbb{E}[|T_0|^2] &= \rho_b\Bigg(\sum_{w=1}^{N_{bs}}\sqrt{\eta_{wo}}\mathcal{G}_{o,b}(z_{wo})\mathbb{E}[\hat{\mathbf{g}}_{wo}^T\hat{\mathbf{g}}_{wo}^*]s_o\Bigg)^2,\\
\mathbb{E}[|T_1|^2] &= \mathbb{E}[|\sum_{w=1}^{N_{bs}}\sqrt{\rho_b\eta_{wo}}\mathcal{G}_{o,b}(z_{wo})(\hat{\mathbf{g}}_{wo}^T\hat{\mathbf{g}}_{wo}^*\\
&\quad -\mathbb{E}[\hat{\mathbf{g}}_{wo}^T\hat{\mathbf{g}}_{wo}^*])s_o|^2],\\
\mathbb{E}[|T_2|^2] &= \mathbb{E}[|\sum_{w=1}^{N_{bs}}\sum_{i\neq o}^{K}\sqrt{\rho_b\eta_{wi}}\mathcal{G}_{o,b}(z_{wo})\hat{\mathbf{g}}_{wo}^T\hat{\mathbf{g}}_{wi}^*s_i|^2],\\
\mathbb{E}[|T_3|^2] &= \mathbb{E}[|\sum_{w=1}^{N_{bs}}\sum_{i=1}^{K}\sqrt{\rho_b\eta_{wi}}\mathcal{G}_{o,b}(z_{wo})\tilde{\mathbf{g}}_{wo}^T\hat{\mathbf{g}}_{wi}^*s_i|^2].
\end{aligned} \tag{11}$$

Generally, the coverage probability is defined as the probability that the SINR of the typical user is greater than a predefined threshold θ, and the rate coverage is defined as the achievable rate of the typical user is greater than a given threshold γ.

Definition 2 (Coverage Probability and Rate Coverage): The downlink coverage probability of a CF-mMIMO user is given as

$$P_{\mathrm{cov}}(\theta) = \mathbb{E}[\mathbb{P}(\mathrm{SINR} > \theta)], \tag{12}$$

and the rate coverage is

$$\mathrm{Ra}^{\mathrm{cf}} = \mathbb{E}\left[\mathbb{P}\left(\left(1-\frac{\tau_{tr}}{\tau_c}\right)(\log_2(1+\mathrm{SINR}) > \gamma)\right)\right], \tag{13}$$

where the expectation operation is for the randomness of the locations, e.g., Φ_b.

III. Performance Analysis

In this section, we study the downlink performance: coverage probability and rate coverage of the typical user. Before proceeding further, we first derive the expression for the uplink channel estimation vector.

Lemma 1 (Uplink Channel Estimation): The estimated channel and the error, $\hat{\mathbf{g}}_{wk}$ and $\tilde{\mathbf{g}}_{wk}$ are, respectively, given by,

$$\begin{aligned}
\hat{\mathbf{g}}_{wk} &= \beta_{wk}\mathbf{y}_{wk},\\
\tilde{\mathbf{g}}_{wk} &= \mathbf{g}_{wk} - \hat{\mathbf{g}}_{wk},
\end{aligned} \tag{14}$$

in which,

$$\beta_{wk} = \frac{\mathcal{G}_{v,b}(z_{wk})l_{wk}}{\sum_{i=1}^{K} l_{wi}\mathcal{G}_{v,b}^2(z_{wi})|\boldsymbol{\psi}_i^H\boldsymbol{\psi}_k|^2 + \frac{1}{\rho_p\tau_{tr}}}. \tag{15}$$

Besides, we have $\mathbb{E}[\hat{\mathbf{g}}_{wk}] = \mathbf{0}_{N_a\times 1}$, $\mathbb{E}[|\hat{\mathbf{g}}_{wk}|^2] = N_a\mathcal{G}_{v,b}(z_{wk})l_{wk}\beta_{wk}$, $\mathbb{E}[|\hat{\mathbf{g}}_{wk}|^4] = N_a^2\Bigg(2\mathcal{G}_{v,b}^2(z_{wk})l_{wk}^2\beta_{wk}^2 + \beta_{wk}^4\sum_{i=1}^{K}|\boldsymbol{\psi}_i^H\boldsymbol{\psi}_k|^4\mathcal{G}_{v,b}^4(z_{wi})l_{wi}^2\left(\frac{1}{m_c}-1\right)\Bigg)$, where m_c depends on the established LoS/NLoS channel between BS n and user k, $\mathbb{E}[\tilde{\mathbf{g}}_{wk}] = \mathbf{0}_{N_a\times 1}$, and $\mathbb{E}[|\tilde{\mathbf{g}}_{wk}|^2] = N_a\mathcal{G}_{v,b}(z_{wk})\Big(l_{wk}-l_{wk}\beta_{wk}\Big)$.

Proof: See Appendix A. ∎

Remark 1: Different from the Rayleigh fading case, the channel estimation vector does not follow a multi-dimensional complex Normal distribution. Recall that Rayleigh fading is a special case of Nakagami-m fading, therefore, by setting $m_c = 1$ above results become the same as Rayleigh fading scenarios. Compared with Rayleigh fading scenario, Nakagami-m fading is different in the expectation of the fourth moment of $\hat{\mathbf{g}}_{wk}$ or the second moment of $|\hat{\mathbf{g}}_{wk}|^2$ due to the term $(\frac{1}{m_c}-1)$ which is strictly negative and results in a lower variation.

A. Downlink Data Transmission

In the following section, we first derive the received signal based on the beamforming and then compute the coverage probability and achievable rate of the typical user. Recall that we consider both aerial users and ground users, the probability of having a ground user as typical user is $p_{gu} = \frac{\mathcal{N}(\mathbf{gu})}{K}$ and the probability of having an aerial user as typical user is $p_{au} = \frac{\mathcal{N}(\mathbf{au})}{K}$. We first simplify (10) to obtain the SINR at the typical user.

Lemma 2 (SINR at the Typical User): The SINR at the typical user is given by

$$\mathrm{SINR} = \frac{\rho_b N_a^2\Bigg(\sum_{w=1}^{N_{bs}}\sqrt{\eta_{wo}}\mathcal{G}_{o,b}^2(z_{wo})l_{wo}\beta_{wo}\Bigg)^2}{1+I}, \tag{16}$$

where

$$\begin{aligned}
I = \rho_b N_a^2\Bigg(&\sum_{w=1}^{N_{bs}}\sum_{i=1}^{K}\eta_{wi}\mathcal{G}_{o,b}^3(z_{wo})\mathcal{G}_{v_i,b}(z_{wi})l_{wo}l_{wi}\beta_{wi}\\
&+\sum_{w=1}^{N_{bs}}\eta_{wo}\mathcal{G}_{o,b}^2(z_{wo})\beta_{wo}^4\sum_{i=1}^{K}|\boldsymbol{\psi}_i^H\boldsymbol{\psi}_o|^4\\
&\mathcal{G}_{v_i,b}^4(z_{wi})l_{wi}^2\left(\frac{1}{m_l}-1\right)\Bigg).
\end{aligned} \tag{17}$$

Proof: See Appendix B. ∎

In CF-mMIMO network, BSs simultaneously serve all users, therefore, the power constraint at the w-th BS is $\sum_{k=1}^{K}\eta_{wk}\mathbb{E}[|\hat{\mathbf{g}}_{wk}^*|^2] \leq 1$. In this work, we consider that BSs serve users by full and uniform power transmission scheme, that is, $\sqrt{\eta_{wk}} = \frac{1}{\sqrt{K\mathbb{E}[|\hat{\mathbf{g}}_{wk}^*|^2]}} = (KN_a\mathcal{G}_{v_k,b}(z_{wk})l_{wk}\beta_{wk})^{-1/2}$. Consequently, the transmit

Authorized licensed use limited to: Maynooth University Library. Downloaded on September 23,2025 at 15:50:34 UTC from IEEE Xplore. Restrictions apply.

signal at BS w is simplified as

$$\mathbf{x}_w = \sqrt{\rho_b/K}\sum_{k=1}^{K}\frac{\hat{\mathbf{g}}_{wk}^*}{\sqrt{N_a\mathcal{G}_{v_k,b}(z_{wk})l_{wk}\beta_{wk}}}s_k, \tag{18}$$

and SINR of the typical user is given in the following corollary.

Corollary 1 SINR at the Typical User under Uniform Power Transmission Scheme: The SINR at the typical user under the uniform power transmission scheme is

$$\text{SINR} = \frac{\rho_b/KN_a\left(\sum_{w=1}^{N_{bs}}\mathcal{G}_{o,b}^{\frac{3}{2}}(z_{wo})\sqrt{l_{wo}\beta_{wo}}\right)^2}{1+I}, \tag{19}$$

where

$$I = \frac{\rho_b N_a}{K}\Bigg(K\sum_{w=1}^{N_{bs}}\mathcal{G}_{o,b}^3(z_{wo})l_{wo} + \sum_{w=1}^{N_{bs}}\mathcal{G}_{o,b}(z_{wo})\beta_{wo}^3\sum_{i=1}^{K}|\boldsymbol{\psi}_i^H\boldsymbol{\psi}_o|^4\mathcal{G}_{v_i,b}^4(z_{wi})\frac{l_{wi}^2}{l_{wo}}\left(\frac{1}{m_c}-1\right)\Bigg). \tag{20}$$

Remark 2: If we ignore the pilot contamination in the denominator, the interference term becomes,

$$I = \frac{\rho_b N_a}{K}\Bigg(K\sum_{w_b=1}^{N_{bs}}\mathcal{G}_{o,b}^3(z_{wo})l_{wo} + \sum_{w=1}^{N_{bs}}\mathcal{G}_{o,b}^5(z_{wo})\beta_{wo}^3 l_{wo}\left(\frac{1}{m_c}-1\right)\Bigg), \tag{21}$$

and compared to (16), SINR are only functions of the distances to all BSs. In that case, if the total number of users is fixed, e.g., K is fixed, the performance of aerial users does not influence the ground users, and vise versa. The performance of the user is only impacted by the distances to BSs, as well as its height (*recall that $l_{wo} = \max(1, r_{wo}^{-\alpha_c})$, where $r_{wo} = \sqrt{\Delta h_{\{au,gu\}}^2 + z_{wo}^2}$*).

B. Coverage Probability and Rate Coverage

Notice that the SINR of the typical user contains the distances to all BSs, which requires a N_{bs}-fold integration to average it over the locations, and pilot contamination. As demonstrated in Corollary 1 (20), the interference is influenced by the distances to all BSs and users, making it intractable and highly complex in the domain of stochastic geometry. Therefore, to make the analysis tractable, we ignore the effect of pilot contamination, which means we use (21) for subsequent analysis.[1] Consequently, the proposed analysis serves as an upper bound for real-life scenarios, as certain terms in the interference are omitted. In what follows, we propose an approximation, which is similar to the approximation used in [46], [53], to simplify the integration of computing SINR. We use this approximation for two main reasons: (i) we include uplink channel estimation and conjugate beamforming, which implies that in the received signal, randomness stems solely from the locations of BSs, and (ii) both the signal and interference are dependent on the locations of all BSs. Consequently, the commonly used Gamma-distribution-based approximation [4] cannot be applied in this context.

The main idea of the proposed approximation is: the SINR is dominated by contributions from the BS which provides the strongest signal, it may not be the nearest BS, due to the antenna model. Observing that both the signal and the interference terms are functions of $\mathcal{G}_{o,b}^3 l_{no}$, therefore, we need to weigh the BS based on the antenna gain and distance.

Before we derive the approximation, we first introduce some important distance distributions. Let R_l be the distance to the nearest LoS BS and R_n be the distance to the nearest NLoS BS. The cumulative distribution function (CDF) and PDF of R_l and R_n are respectively, given by

$$F_{R_{\{l,n\}}}(r,\lambda) = 1-\exp\left(-2\pi\lambda\int_0^r zP_{\{l,n\}}(\sqrt{\Delta h_v^2+z^2})\mathrm{d}z\right),$$
$$f_{R_{\{l,n\}}}(r,\lambda) = 2\pi\lambda P_{\{l,n\}}(r)r \exp\left(-2\pi\lambda\int_0^r zP_{\{l,n\}}(\sqrt{\Delta h_v^2+z^2})\mathrm{d}z\right). \tag{22}$$

Let $R_{l,m}$ and $R_{n,m}$ be the distances to the nearest LoS BS and NLoS BS that provide the mainlobe gain, respectively. The CDF and PDF of $R_{l,m}$ and $R_{n,m}$ are respectively, given by

$$F_{R_{\{l,n\},m}}(r,\lambda) = \begin{cases} 0, & \text{if} \quad r < z_{b,1}, \\ 1-\exp\left(-2\pi\lambda\int_{z_{b,1}}^r zP_{\{l,n\}}(\sqrt{\Delta h_v^2+z^2})\mathrm{d}z\right), & \\ \quad \text{if} \quad z_{b,1} < r < z_{b,2}, & \\ 1-\exp\left(-2\pi\lambda\int_{z_{b,1}}^{z_{b,2}} zP_{\{l,n\}}(\sqrt{\Delta h_v^2+z^2})\mathrm{d}z\right), & \\ \quad \text{if} \quad z_{b,2} < r, & \end{cases} \tag{23}$$

$$f_{R_{\{l,n\},m}}(r,\lambda) = \begin{cases} 2\pi\lambda P_{\{l,n\}}(r)r\exp\left(-2\pi\lambda\int_{z_{b,1}}^r z \right. & \\ \left. \times P_{\{l,n\}}(\sqrt{\Delta h_v^2+z^2})\mathrm{d}z\right), \quad \text{if} \quad z_{b,1} < r < z_{b,2}, & \\ 0, \quad \text{otherwise}, & \end{cases} \tag{24}$$

The above CDFs and PDFs are obtained by using the properties of non-homogenous PPP [4].

Let $b_{ub} \in \Phi_{b,ub}$ and $b_{db} \in \Phi_{b,db}$ be the locations of the up-tilted and down-tilted BSs, respectively. For the typical user, (if the typical user is an aerial user then $g = ub$ and if the typical user is a ground user then $g = db$) the strongest LoS BS and NLoS BS have the following four cases, respectively: (i) the strongest LoS BS can be a b_{ub} or b_{db} within $B(0, z_{g,1})$

[1]Pilot contamination is a complex engineering challenge caused by various factors, such as hardware impairments, non-reciprocal transceivers, and limitations in coherence time. It is also influenced by the transmission scheme, whether time or frequency division duplex, and by whether the transmission is uplink or downlink. Therefore, it can be an interesting future direction.

Authorized licensed use limited to: Maynooth University Library. Downloaded on September 23,2025 at 15:50:34 UTC from IEEE Xplore. Restrictions apply.

with probability $p_{\text{los},1}$, be a b_{ub} within $B(0, z_{g,1} - z_{g,2})$ with probability $p_{\text{los},2}$, be a b_{db} within $B(0, z_{g,1} - z_{g,2})$ with probability $p_{\text{los},3}$, and be a b_{ub} or b_{db} outside $B(0, z_{g,2})$ with probability $p_{\text{los},4}$; (ii) the strongest NLoS BS can be a b_{ub} or b_{db} within $B(0, z_{g,1})$ with probability $p_{\text{nlos},1}$, be a b_{ub} within $B(0, z_{g,1} - z_{g,2})$ with probability $p_{\text{nlos},2}$, be a b_{db} within $B(0, z_{g,1} - z_{g,2})$ with probability $p_{\text{nlos},3}$, and be a b_{ub} or b_{db} outside $B(0, z_{g,2})$ with probability $p_{\text{nlos},4}$. Each of the probabilities $p_{\{\text{los,nlos}\},\{1,2,3,4\}}$ are defined in the below lemma.

Lemma 3 (Strongest BS Events): The probabilities of the above events are, respectively, given by

$$\begin{aligned}
p_{\{\text{los,nlos}\},1} &= f_{R_{\{l,n\}}}(r, \lambda_b)\bar{F}_{R_{\{l,n\},m}}(d_l(r), \lambda_{b,g}),\\
p_{\{\text{los,nlos}\},2} &= \bar{F}_{R_{\{l,n\}}}(d'_l(r), \lambda_b) f_{R_{\{l,n\},m}}(r, \lambda_{b,g}),\\
p_{\{\text{los,nlos}\},3} &= \bar{F}_{R_{\{l,n\}}}(\sqrt{z_{g,1}^2 + \Delta h_o^2}, \lambda_b)\bar{F}_{R_{\{l,n\}}}(d_l(r), \lambda_{b,g})\\
&\quad F_{R_{\{l,n\},m}}(r, (\lambda_b - \lambda_{b,g})),\\
p_{\{\text{los,nlos}\},4} &= f_{R_{\{l,n\}}}(r, \lambda_b),
\end{aligned} \tag{25}$$

in which,

$$d_{\{l,n\}}(r) = \min\left(\sqrt{z_{g,2}^2 + \Delta h_o^2}, \max\left(\zeta_m^{\frac{3}{\alpha_{\{l,n\}}}} r, \sqrt{z_{g,1}^2 + \Delta h_o^2}\right)\right), \tag{26}$$

$$d'_{\{l,n\}}(r) = \min\left(\sqrt{z_{g,1}^2 + \Delta h_o^2}, \max\left(\zeta_m^{-\frac{3}{\alpha_{\{l,n\}}}} r, \Delta h_o\right)\right). \tag{27}$$

Proof: See Appendix C. ∎

In each case defined above, the SINR at the typical user is approximated by summing of the exact term of the signal from strongest LoS and NLoS BS and the mean of the remaining BSs. Let r_l and r_n represent the distances to the LoS and NLoS BSs providing the strongest signal, considering both distance and antenna gain (a similar concept is used in [54]). The approximated SINR is given in the following lemma.

Lemma 4 (Approximated SINR): Given the location of the BS providing the strongest signal, the SINR at the typical user is approximated by

$$\overline{\text{SINR}}(r_l, r_n) \approx \frac{(\text{S}_{l,i}(r_l) + \text{S}_{n,j}(r_n))^2}{\frac{K}{N_a \rho_p} + \text{I}_{l,i} + \text{I}_{n,j}}, \tag{28}$$

where $i \in \{1,2,3,4\}$ and $j \in \{1,2,3,4\}$ correspond to the locations of strongest LoS and NLoS BSs as defined above Lemma 3, respectively, and

$$\begin{aligned}
\text{S}_{\{l,n\},1}(r_{\{l,n\}}) &\approx \frac{(r_{\{l,n\}})^{-\alpha_{\{l,n\}}}}{\sqrt{(r_{\{l,n\}})^{-\alpha_{\{l,n\}}} + \frac{1}{\rho_p \tau_{tr}}}}\\
&+ 2\pi\lambda_b \int_{r_{\{l,n\}}}^{\sqrt{z_{ub,1}^2 + \Delta h_o^2}} f_1(r) r \mathrm{d}r\\
&+ 2\pi\lambda_{b,ub} \int_{d'_{\{l,n\}}(r_{\{l,n\}})}^{\sqrt{z_{ub,2}^2 + \Delta h_o^2}} f_2(r) r \mathrm{d}r\\
&+ 2\pi\lambda_b \int_{\sqrt{z_{ub,2}^2 + \Delta h_o^2}}^{\infty} f_1(r) r \mathrm{d}r\\
&+ 2\pi\lambda_{b,d} \int_{\sqrt{z_{ub,1}^2 + \Delta h_o^2}}^{\sqrt{z_{ub,2}^2 + \Delta h_o^2}} f_1(r) r \mathrm{d}r,
\end{aligned} \tag{29}$$

$$\begin{aligned}
\text{S}_{\{l,n\},2}(r_{\{l,n\}}) &\approx \frac{\zeta_m^{\frac{3}{2}} r^{-\alpha_{\{l,n\}}}}{\sqrt{r^{-\alpha_{\{l,n\}}} + \frac{1}{\rho_p \tau_{tr}}}}\\
&+ 2\pi\lambda_b \int_{\min(d_{\{l,n\}}(r_{\{l,n\}}), \sqrt{z_{ub,1}^2 + \Delta h_o^2})}^{\sqrt{z_{ub,1}^2 + \Delta h_o^2}} f_1(r) r \mathrm{d}r\\
&+ 2\pi\lambda_{b,ub} \int_{r_{\{l,n\}}}^{\sqrt{z_{ub,2}^2 + \Delta h_o^2}} f_2(r) r \mathrm{d}r\\
&+ 2\pi\lambda_b \int_{\sqrt{z_{ub,2}^2 + \Delta h_o^2}}^{\infty} f_1(r) r \mathrm{d}r\\
&+ 2\pi\lambda_{b,db} \int_{d_{\{l,n\}}(r_{\{l,n\}})}^{\sqrt{z_{ub,2}^2 + h_o^2}} f_1(r) r \mathrm{d}r,
\end{aligned} \tag{30}$$

$$\begin{aligned}
&\text{S}_{\{l,n\},3}(r_{\{l,n\}})\\
&\approx \frac{r^{-\alpha_{\{l,n\}}}}{\sqrt{r^{-\alpha_{\{l,n\}}} + \frac{1}{\rho_p \tau_{tr}}}}\\
&+ 2\pi\lambda_{b,ub} \int_{d'_{\{l,n\}}(r_{\{l,n\}})}^{\sqrt{z_{ub,2}^2 + \Delta h_o^2}} f_2(r) r \mathrm{d}r\\
&+ 2\pi\lambda_{b,ub} \int_{\sqrt{z_{ub,2}^2 + \Delta h_o^2}}^{\infty} f_1(r) r \mathrm{d}r\\
&+ 2\pi\lambda_{b,db} \int_{r_{\{l,n\}}}^{\infty} f_1(r) r \mathrm{d}r,
\end{aligned} \tag{31}$$

$$\begin{aligned}
\text{S}_{\{l,n\},4}(r_{\{l,n\}}) &\approx \frac{r^{-\alpha_{\{l,n\}}}}{\sqrt{r^{-\alpha_{\{l,n\}}} + \frac{1}{\rho_p \tau_{tr}}}}\\
&+ 2\pi\lambda_b \int_{r_{\{l,n\}}}^{\infty} f_1(r) r \mathrm{d}r,
\end{aligned} \tag{32}$$

in which

$$\begin{aligned}
f_1(r) &= \frac{P_{\{l,n\}}(r) r^{-\alpha_{\{l,n\}}}}{\sqrt{r^{-\alpha_{\{l,n\}}} + \frac{1}{\rho_p \tau_{tr}}}},\\
f_2(r) &= \frac{P_{\{l,n\}}(r) \zeta_m^2 r^{-\alpha_{\{l,n\}}}}{\sqrt{\zeta_m^2 r^{-\alpha_{\{l,n\}}} + \frac{1}{\rho_p \tau_{tr}}}},
\end{aligned} \tag{33}$$

similarly, the interference terms are given by,

$$\begin{aligned}
\text{I}_{\{l,n\},1} &\approx K l_{\{l,n\}o} + \beta_{\{l,n\}o}^3 l_{\{l,n\}o}\left(\frac{1}{m_{\{l,n\}}} - 1\right) + 2\pi\\
&\times \left(\lambda_b \int_{r_{\{l,n\}}}^{\sqrt{z_{ub,1}^2 + \Delta h_o^2}} f_3(r) r \mathrm{d}r\right.\\
&+ \lambda_{b,ub} \int_{d'_{\{l,n\}}(r_{\{l,n\}})}^{\sqrt{z_{ub,2}^2 + \Delta h_o^2}} f_4(r) r \mathrm{d}r\\
&\left.+ \lambda_b \int_{\sqrt{z_{ub,2}^2 + h_o^2}}^{\infty} f_3(r) r \mathrm{d}r + \lambda_{b,db} \int_{\sqrt{z_{ub,1}^2 + \Delta h_o^2}}^{\sqrt{z_{ub,2}^2 + \Delta h_o^2}} f_3(r) r \mathrm{d}r\right),
\end{aligned} \tag{34}$$

$$\text{I}_{\{l,n\},2} \approx K\zeta_m^3 l_{\{l,n\}o} + \zeta_m^5 \beta_{\{l,n\}o}^3 l_{\{l,n\}o}\left(\frac{1}{m_{\{l,n\}}} - 1\right)$$

Authorized licensed use limited to: Maynooth University Library. Downloaded on September 23,2025 at 15:50:34 UTC from IEEE Xplore. Restrictions apply.

$$+2\pi\Bigg(\lambda_b\int_{\min(d_{\{l,n\}}(r_{\{l,n\}}),\sqrt{z_{ub,1}^2+\Delta h_o^2})}^{\sqrt{z_{ub,1}^2+\Delta h_o^2}} f_3(r)r\mathrm{d}r + \lambda_{b,ub}\int_{r_{\{l,n\}}}^{\sqrt{z_{ub,2}^2+\Delta h_o^2}} f_4(r)r\mathrm{d}r + \lambda_b\int_{\sqrt{z_{ub,2}^2+\Delta h_o^2}}^{\infty} f_3(r)r\mathrm{d}r + \lambda_{b,db}\int_{d_{\{l,n\}}(r_{\{l,n\}})}^{\sqrt{z_{ub,2}^2+\Delta h_o^2}} f_3(r)r\mathrm{d}r\Bigg), \tag{35}$$

$$\mathrm{I}_{\{l,n\},3} \approx Kl_{\{l,n\}o} + \beta_{\{l,n\}o}^3 l_{\{l,n\}o}\left(\frac{1}{m_{\{l,n\}}}-1\right) + 2\pi\lambda_{b,ub}\int_{d'_{\{l,n\}}(r_{\{l,n\}})}^{\sqrt{z_{ub,2}^2+\Delta h_o^2}} f_4(r)r\mathrm{d}r + 2\pi\lambda_{b,ub}\int_{\sqrt{z_{ub,2}^2+\Delta h_o^2}}^{\infty} f_3(r)r\mathrm{d}r + 2\pi\lambda_{b,db}\int_{r_o}^{\infty} f_3(r)r\mathrm{d}r, \tag{36}$$

$$\mathrm{I}_{\{l,n\},4} \approx Kl_{\{l,n\}o} + \beta_{\{l,n\}o}^3 l_{\{l,n\}o}\left(\frac{1}{m_{\{l,n\}}}-1\right) + 2\pi\lambda_b\int_{r_{\{l,n\}}}^{\infty} f_3(r)r\mathrm{d}r, \tag{37}$$

in which

$$f_3(r) = P_{\{l,n\}}(r)r\left[Kr^{-\alpha_{\{l,n\}}} + \frac{r^{-4\alpha_{\{l,n\}}}\left(\frac{1}{m_{\{l,n\}}}-1\right)}{\left(r^{-\alpha_{\{l,n\}}}+\frac{1}{\rho_p\tau_{tr}}\right)^3}\right],$$
$$f_4(r) = P_{\{l,n\}}(r)r\left[K\zeta_m^3 r^{-\alpha_{\{l,n\}}} + \frac{\zeta_m^8 r^{-4\alpha_{\{l,n\}}}\left(\frac{1}{m_{\{l,n\}}}-1\right)}{\left(\zeta_m^2 r^{-\alpha_{\{l,n\}}}+\frac{1}{\rho_p\tau_{tr}}\right)^3}\right]. \tag{38}$$

Proof: See Appendix D. ∎

Consequently, the coverage probability and rate coverage of the typical user are obtained by taking the expectation over the locations of the strongest LoS/NLoS BSs, given in the following theorem. Recall that p_{au} and p_{gu} are the probabilities of the typical user being aerial or ground, respectively.

Theorem 1 (Coverage Probability and Rate Coverage): The coverage probability of the typical user is

$$P_{\mathrm{cov}}(\theta) = p_{au}P_{\mathrm{cov,au}}(\theta) + p_{gu}P_{\mathrm{cov,gu}}(\theta), \tag{39}$$

where $P_{\mathrm{cov,au}}(\theta)$ and $P_{\mathrm{cov,gu}}(\theta)$ are the coverage probability of the aerial user and ground user, respectively, given by

$$P_{\mathrm{cov},\{\mathrm{au,gu}\}}(\theta) = \sum_{i=1}^{4}\sum_{j=1}^{4}\int_{r_{l,\{au,gu\}}}\int_{r_{n,\{au,gu\}}} p_{\mathrm{los,i}}(r_{l,\{au,gu\}})p_{\mathrm{nlos,j}}(r_{n,\{au,gu\}}) \times \mathbb{1}(\overline{\mathrm{SINR}}(r_{l,\{au,gu\}},r_{n,\{au,gu\}})>\theta)\,\mathrm{d}r_{n,\{au,gu\}}\mathrm{d}r_{l,\{au,gu\}}, \tag{40}$$

and the rate coverage is

$$\mathrm{Ra}^{\mathrm{cf}}(\gamma) = p_{au}\mathrm{Ra}_{au}^{\mathrm{cf}}(\gamma) + p_{gu}\mathrm{Ra}_{gu}^{\mathrm{cf}}(\gamma), \tag{41}$$

where $\mathrm{Ra}_{au}^{\mathrm{cf}}(\theta)$ and $\mathrm{Ra}_{gu}^{\mathrm{cf}}(\theta)$ are the rate coverage of the aerial user and ground user, respectively, given by

$$\mathrm{Ra}_{\{au,gu\}}^{\mathrm{cf}}(\gamma) = \sum_{i=1}^{4}\sum_{j=1}^{4}\int_{r_{l,\{au,gu\}}}\int_{r_{n,\{au,gu\}}} p_{\mathrm{los,i}}(r_{l,\{au,gu\}}) \times p_{\mathrm{nlos,j}}(r_{n,\{au,gu\}})\mathbb{1}(\log_2(1+\overline{\mathrm{SINR}}(r_{l,\{au,gu\}},r_{n,\{au,gu\}})) > \gamma)\left(1-\frac{\tau_{tr}}{\tau_c}\right)\mathrm{d}r_{n,\{au,gu\}}\mathrm{d}r_{l,\{au,gu\}}, \tag{42}$$

where the subscript $\{au,gu\}$ denotes the aerial and ground users, and they are different when computing the integration due to the altitudes.

In the next subsection, we consider a special case, where omnidirection antenna model is considered, and all users experience the same antenna gain $\zeta_m = \zeta_s = 1$ from all BSs.

C. Special Case

In the case of omnidirectional antenna, antenna gain equals to 1 and the SINR in (19) becomes

$$\overline{\mathrm{SINR}}_{\mathrm{omni}} = \frac{\rho_b\left(\sum_{w=1}^{N_{bs}}\sqrt{\eta_{wo}}N_a l_{wo}\beta_{wo}\right)^2}{1+I}. \tag{43}$$

where,

$$I = \rho_b\sum_{w=1}^{N_{bs}}\sum_{k=1}^{K}\eta_{wk}N_a^2 l_{wk}\beta_{wk}l_{wo} + \rho_p\sum_{w=1}^{N_{bs}}\eta_{wo}N_a^2\beta_{wo}^4\sum_{i=1}^{K}|\boldsymbol{\psi}_i^H\boldsymbol{\psi}_o|^4 l_{wi}^2\left(\frac{1}{m_l}-1\right). \tag{44}$$

Similarly, we consider full and uniform power transmission: $\sqrt{\eta_{wk}} = \frac{1}{\sqrt{K\mathbb{E}[|\hat{\mathbf{g}}_{wk}^*|^2]}} = (KN_a l_{wk}\beta_{wk})^{-1/2}$, the SINR at the typical user is

$$\overline{\mathrm{SINR}}_{\mathrm{omni}} = \frac{\left(\sum_{w=1}^{N_{bs}}\sqrt{l_{wo}\beta_{wo}}\right)^2}{\frac{K}{N_a\rho_p} + K\sum_{w=1}^{N_{bs}}l_{wo} + \sum_{w=1}^{N_{bs}}\beta_{wo}^3 l_{wo}\left(\frac{1}{m_l}-1\right)}. \tag{45}$$

In the case of omnidirectional antenna, the nearest BS provides the strongest component to the SINR. Under the this observation, we approximate the SINR at the typical user as the sum of the exact terms of the nearest LoS and NLoS BS and the mean of the rest of BSs.

Corollary 2 (Approximated SINR): If the antenna is omnidirectional, the SINR at the typical user is

$$\overline{\mathrm{SINR}}_{\mathrm{omni}}(R_l,R_n) \approx \frac{\left(\frac{R_l^{-\alpha_l}}{\sqrt{R_l^{-\alpha_l}+\frac{1}{\rho_p\tau_{tr}}}} + \frac{R_n^{-\alpha_n}}{\sqrt{R_n^{-\alpha_n}+\frac{1}{\rho_p\tau_{tr}}}} + 2\pi\lambda_b(\kappa_l(R_l)+\kappa_l(R_n))\right)^2}{\frac{K}{N_a\rho_p} + K(R_l^{-\alpha_l}+r_n^{-\alpha_n}) + \frac{R_l^{-4\alpha_l}\left(\frac{1}{m_l}-1\right)}{\left(R_l^{-\alpha_l}+\frac{1}{\rho_p\tau_{tr}}\right)^3} + \kappa_1(R_l) + \kappa_2(R_n)}, \tag{46}$$

Authorized licensed use limited to: Maynooth University Library. Downloaded on September 23,2025 at 15:50:34 UTC from IEEE Xplore. Restrictions apply.

where

$$\kappa_l(r_o) = \int_{r_o}^{\infty} P_l(r) \frac{r^{-\alpha_l}}{\sqrt{r^{-\alpha_l} + \frac{1}{\rho_p \tau_{tr}}}} r\mathrm{d}r,$$
$$\kappa_n(r_o) = \int_{r_o}^{\infty} P_n(r) \frac{r^{-\alpha_n}}{\sqrt{r^{-\alpha_n} + \frac{1}{\rho_p \tau_{tr}}}} r\mathrm{d}r,$$
$$\kappa_1(r_o) = \int_{r_o}^{\infty} P_l(r) \left[K r^{-\alpha_l} + \frac{r^{-4\alpha_l}(\frac{1}{m_l} - 1)}{(r^{-\alpha_l} + \frac{1}{\rho_p \tau_{tr}})^3} \right] r\mathrm{d}r,$$
$$\kappa_2(r_o) = \int_{r_o}^{\infty} P_n(r) K r^{-\alpha_n} r\mathrm{d}r. \quad (47)$$

Proof: See Appendix E. ∎

After obtaining the approximated SINR, the coverage probability and rate coverage are derived by substituting (46) into (40) and (42), and taking the expectation over R_l and R_n, whose PDFs are given in (22) with $\lambda = \lambda_b$.

D. Small Cell

For the sake of comparison, we consider a small cell system model with the same BS density and number of users. Each BS serves only one user at a time, the user associates with the available BS that provides the strongest signal (maximum ratio combining), and the BSs which have no associated users remain silent. Note that the BS that provides the strongest signal is obtained by jointly considering the LoS/NLoS transmission and distances to the user. Therefore, the interference comes from the active BSs, the BSs that are serving users. Let b_k be the BS chosen by the user k, then we have

$$b_k = \arg\ \max_{i \in \{\text{available BSs}\}} \mathbf{g}_{b_i k}, \quad (48)$$

in which $\mathbf{g}_{b_i k} \in N_a \times 1$ since we assume the same number of antennas as CF-mMIMO system model. In small cell system, we only compute the omnidirectional antenna scenario. For the dedicated BS scenario please refer to [13] for details.

In the downlink transmission, the user estimate the channel based on the pilot sent by the BSs and similar to CF-mMIMO, the minimum mean square error estimation of the channel is

$$\hat{\mathbf{g}}_{b_k k} = \mathbf{g}_{b_k k} - \tilde{\mathbf{g}}_{b_k k}, \quad (49)$$

in which $\tilde{\mathbf{g}}_{b_k k}$ is the channel estimation error. Besides, we have $\mathbb{E}[||\hat{\mathbf{g}}_{b_k k}||^2] = N_a l_{b_k k} \beta_{b_k k}$ and $\mathbb{E}[||\tilde{\mathbf{g}}_{b_k k}||^2] = N_a (l_{b_k k} - l_{nk} \beta^{sc}_{b_k k})$, where

$$\beta^{sc}_{b_k k} = \frac{l_{b_k k}}{\sum_{i=1}^{K} l_{b_k i} |\boldsymbol{\psi}_i^H \boldsymbol{\psi}_k|^2 + \frac{1}{\rho_d^{sc} \tau_{tr,d}^{sc}}}, \quad (50)$$

in which ρ_d^{sc} and $\tau_{tr,d}^{sc}$ denote SNR of downlink transmission and downlink training duration in samples, respectively. Assuming the BS using the full power to serve the user, consequently, the received power at the user k is

$$y_k = \sqrt{\rho_d^{sc}} \hat{\mathbf{g}}_{b_k k} s_k + \sqrt{\rho_d^{sc}} \sum_{k' \neq k}^{K} \mathbf{g}_{b_{k'} k} s_{k'} + \sqrt{\rho_d^{sc}} \tilde{\mathbf{g}}_{b_k k} s_k + n_k^{sc}, \quad (51)$$

where $n_k^{sc} \sim \mathcal{CN}(0,1)$ is the additive Gaussian noise. Consequently, the coverage probability and achievable rate of small cell users are given in the following equations,

$$P_{\text{cov}}^{\text{sc}}(\theta) = \mathbb{E}[\mathbb{P}(\text{SINR}^{\text{sc}} > \theta)], \quad (52)$$

$$\text{Ra}^{\text{sc}}(\gamma) = \mathbb{E}\left[\mathbb{P}\left(\left(1 - \frac{\tau_{tr,u}^{sc} + \tau_{tr,d}^{sc}}{\tau_c} \right) \log(\text{SINR}^{\text{sc}} + 1) > \gamma \right) \right], \quad (53)$$

where SINR^{sc} denotes the SINR of small cell user,

$$\text{SINR}^{\text{sc}} = \frac{||\hat{\mathbf{g}}_{b_k k}||^2}{\sum_{k' \neq n} ||\mathbf{g}_{b_{k'} k}||^2 + ||\tilde{\mathbf{g}}_{b_k k}||^2 + \frac{1}{\rho_d^{sc} \tau_{tr,d}^{sc}}}. \quad (54)$$

Compared to CF-mMIMO system, the rate coverage of small cell system is slightly different since it requires one more downlink training phase.

Since the number of users is fixed, the corresponding number of serving BSs is fixed. Therefore, for a user, the interfering BSs form a BPP. Due to the correlation on the locations of users (since users choose their serving BSs at a random order), the $\text{SINR}_i^{\text{sc}}$ and data rate, Ra_i^{sc}, of small cell a user are solved by the Algorithm 1, and consequently, (52) and (53) are obtained by averaging over the realization of Φ_b.

Algorithm 1 Algorithm for Small Cell SINR and Data Rate

1: Let $\Phi_b' = \Phi_b$
2: **for** $k \leq K$ **do**
3: Choose $b_k = \arg\ \max \mathbf{g}_{b_i k}$, in which $b_i \in \Phi_b'$
4: $\Phi_b' = \Phi_b' \setminus \{b_k\}$
5: **end for**
6: Compute the $\text{SINR}_i^{\text{sc}}$ and Ra_i^{sc} for a random user $i \in K$

In Algorithm 1, Φ_b' denotes the locations of the available BSs. Since we assume one BS can only serve one user in small cell systems, once a BS associates with a user it becomes unavailable, e.g., $\Phi_b' = \Phi_b' \setminus \{b_k\}$.

IV. Numerical Results

In this section, we aim to validate our analytical results with simulations and reveal multiple useful system-level insights. Additionally, we provide comparisons between CF-mMIMO and small cell systems to illustrate the scenarios under which CF-mMIMO performs better. To ensure a fair comparison between the CF-mMIMO systems and small cell systems, the total radiated power is set to be equal in both architectures. That is, we have $\rho_{b,sc} = \frac{N_{bs}}{K} \rho_b$. Furthermore, we set $\tau_{tr,d}^{sc} = \tau_{tr,u}^{sc} = \tau_{tr}$. Additionally, we consider a finite circular region of radius r_s. Unless stated otherwise, we use the simulation parameters as listed in Table II.

For the simulations of the given system setup, for each iteration, we first generate two independent realizations of a PPP and a BPP for the locations of BSs and users (the total number of users is K), respectively. Then, we use independent thinning to obtain δ up-tilted BSs and $(1-\delta)$ down-tilted BSs,

Authorized licensed use limited to: Maynooth University Library. Downloaded on September 23,2025 at 15:50:34 UTC from IEEE Xplore. Restrictions apply.

TABLE II
TABLE OF PARAMETERS

Parameter	Symbol	Simulation Value
Density of BS	λ_b	40 BS/km^2
Number of users, number of antennas	K, N_a	30, 5
Uplink pilot SNR	ρ_p	112 dB
Downlink SNR	ρ_b	122 dB
Bandwidth and noise power	b_w, σ^2	20 MHz, -92 dBm
Orthogonal pilot sequence length, coherence block length	τ_{tr}, τ_c	20, 200
Antenna gain	ζ_m, ζ_s	10 dB, 0 dB
Antenna angles	$\phi_{db}, \phi_{ub}, \theta_{db}, \theta_{ub}$	$(20, 20)^\circ$, $(12, 12)^\circ$
Environment parameters (highrise urban area)	(e_1, e_2)	$(27, 0.08)$
Environment parameters (dense urban area)	(e_1, e_2)	$(12, 0.11)$
Environment parameters (suburban urban area)	(e_1, e_2)	$(9.6, 0.16)$
Environment parameters (urban area)	(e_1, e_2)	$(4.88, 0.43)$
N/LoS path-loss exponent	α_n, α_l	$4, 2.1$
N/LoS fading gain	m_n, m_l	$1, 3$
Simulation window	r_s	1 km
UAV altitude	Δh_{au}	100 m

as well as $\mathcal{N}(\mathbf{au}) = 20$ aerial users and $\mathcal{N}(\mathbf{gu}) = 10$ ground users. Next, minimum mean square error channel estimation is used to estimate the channel between each user and BS. Therefore, in each iteration, we (i) randomly select one user as the typical user, (ii) generate a set of Gamma random variables as channel fading, and (iii) compute the SINR of the typical user based on Equation (10). Iterations are repeated for a large number until the curve is smooth.

Firstly, we would like to show the coverage performance of aerial users in CF-mMIMO networks. We first plot Fig. 2 to show the tightness of the approximation proposed in Lemma 4 against the SINR in the case of aerial users $\Delta h_{au} = 100$ m. The proposed approximation shows a good matching at large values of r_s and we observe that the proposed approximation cannot capture the smooth transition in the value of coverage probability at some values of θ. As mentioned, the proposed approximation is obtained by accurately considering the dominant signal while averaging the remaining terms. Therefore, given the location of the BS that provides the strongest signal, the coverage performance of the typical user is determined (as the remaining terms are based on the location of the dominant-signal BS). However, in the simulation, the coverage performance of the typical user is not determined due to the effect of the second-dominant BS. In other words, the performance at the smooth transition part can be improved by accurately considering the locations of the second/third/... dominant BSs.

In Fig. 2 (a) shows the influence of simulation areas and Nakagami-m fading parameters on the aerial user performance. We set $K = 1$ which refers to all BSs serving only one aerial user, as the performance of the aerial user is the main focus and contribution of this work. Additionally, since we proposed an approximation, we need to demonstrate the accuracy of this approximation under different system parameters, such as Nakagami-m fading. Comparing LoS and NLoS users, the difference is mainly caused by the second term in the denominator of (21) as well as the path loss exponent. The value of this term is comparatively low, which is β to the power of 3, but has a high influence at the tails of SINR. However, we can expect that this term has a low impact on the system performance at a large number of users since we assume a uniform power allocation and K is directly multiplied by the first term of the interference, see (21), and this conclusion validates in Fig. 2 (b). In Fig. 2 (b) we consider a realistic scenario in

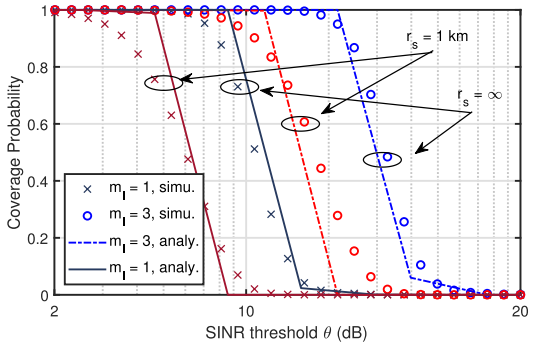

(a)

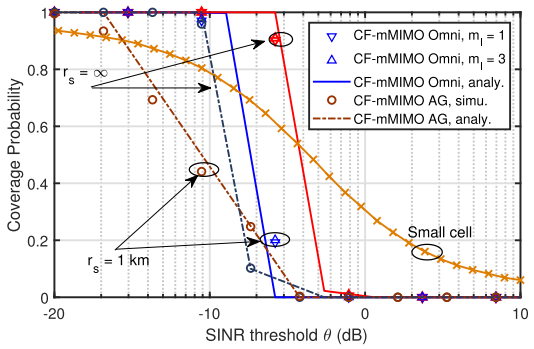

(b)

Fig. 2. (Aerial user only) Simulation and analysis results of coverage probability of aerial users $\Delta h_{au} = 100$ m for both CF-mMIMO and small cell systems: **(a)** Coverage probability under $K = 1$ and different values of m_l and r_s, **(b)** Coverage probability under $K = 30$, up-tilted/down-tilted antennas, in which $\delta = 0.3$, and different values of m_l and r_s. 'AG' refers to dedicated aerial antenna.

which $K = 30$, we compare the coverage performance of users in the case of small cell, dedicated aerial antenna (referred to as 'AG' in the figure) with $\delta = 0.3$ and omnidirectional antenna scenarios. Compared with our previous work [13], in which we show that the aerial dedicated antenna can improve the system coverage performance, the aerial dedicated antenna cannot improve the coverage performance in the CF-mMIMO scenario. This is because the received signal from a BS contains both the desired signal and the interference (since the BS simultaneously serves all the users). As shown in (19) in Cor. 1, the SINR of the typical user is a ratio between the square of the summation of the distances to all BSs and the summation of the square of distances to all BSs. Besides, we compare the coverage performance between small cell and CF-mMIMO systems, in which r_s of the small cell is set at 1 km.

The results in Fig. 2 (b) show that the CF-mMIMO system provides users with uniform performance. The SINR of users is concentrated, as evidenced by the sharp decrease in the complementary cumulative distribution function (CCDF) of coverage probability, indicating that users achieve similar SINR. In contrast, in the small cell system, the SINR of users varies dramatically, with the CCDF of coverage probability decreasing slowly. This implies that while some users achieve high SINR, others have low SINR. Additionally, the minimum achievable SINR, defined as the minimum SINR that users

Authorized licensed use limited to: Maynooth University Library. Downloaded on September 23,2025 at 15:50:34 UTC from IEEE Xplore. Restrictions apply.

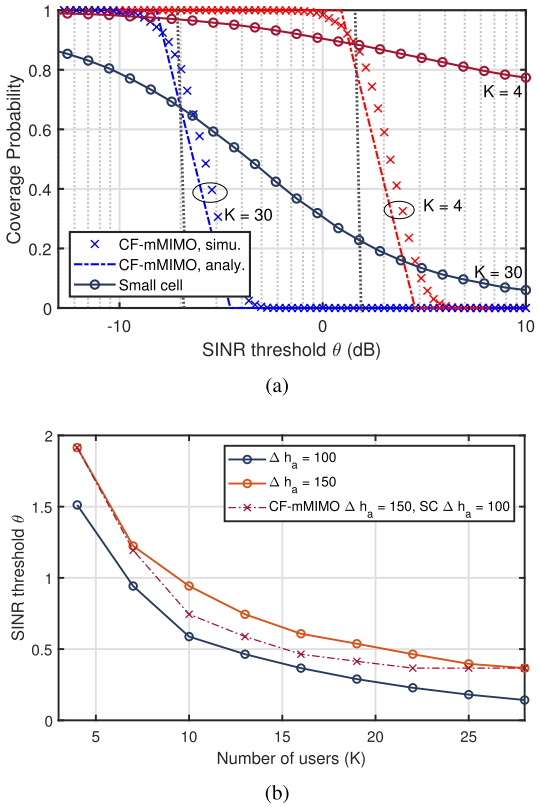

Fig. 3. **(a)** Analysis and simulation results of coverage probability of CF-mMIMO and small cell systems under different number of aerial users. **(b)** The intersection points in **(a)**.

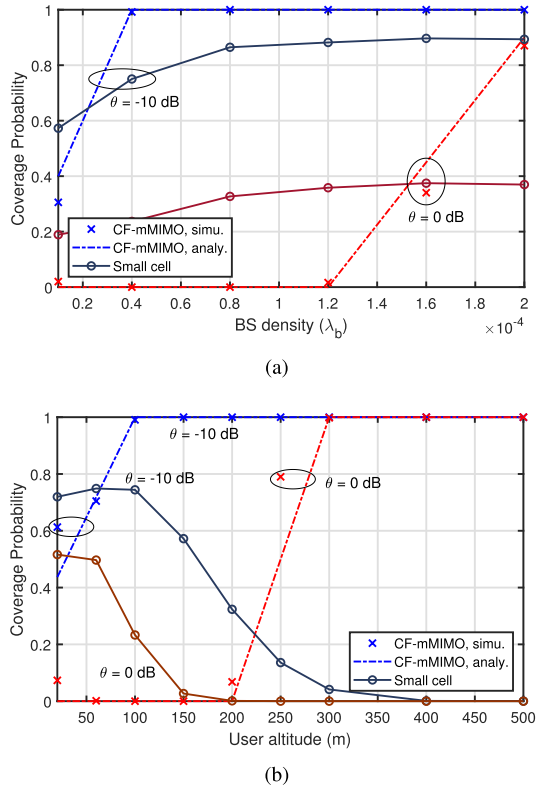

Fig. 4. Analysis and simulation results of coverage probability of CF-mMIMO and small cell systems under: **(a)** different BS densities, and **(b)** user altitudes.

can achieve with probability 1, of the CF-mMIMO system is much higher than that of the small cell system. For example, the minimum SINR is about -10 dB in CF-mMIMO systems, while it is less than -20 dB in small cell networks, as shown in Fig. 2 (b). Since we observe that up-tilted/down-tilted antennas cannot improve system performance compared to omnidirectional antennas, in the following figures, we focus on the CF-mMIMO performance under the omnidirectional antenna case. Here, the antenna gain is fixed at 1, and the BS that provides the strongest received power is obtained by jointly considering the LoS/NLoS transmission and distances to users.

In Fig. 3 (a), we plot the analysis and simulation results of CF-mMIMO and small cell systems under different numbers of aerial users and $\Delta h_{au} = 100$ m. The coverage probability of small cell users decreases with the increasing number of users due to further distance to the available BSs and a higher probability of having interferer BSs that are closer than the serving BS. For the CF-mMIMO user, the performance decreases with the increasing of K due to the desired signal from one BS decreases, and as shown in (46), the interference is obtained by K times the summation of the distances.

In Fig. 3 (b), we plot the SINR threshold below which the CF-mMIMO system performs better than the small cell system (which is obtained by finding the intersect points in Fig. 3 (a)). We compare three different scenarios: (i) aerial users are deployed at the same altitude at $\Delta h_{au} = 100$, (ii) aerial users are deployed at the same altitude at $\Delta h_{au} = 150$, and (iii) the aerial users are deployed at the different altitude, $\Delta h_{au} = 150$ for CF-mMIMO users and $\Delta h_{au} = 100$ for small cell users, since the performance of small cell users decreases with the increase of the user altitude and the optimal altitude of small cell user is around 100 m. We show that CF-mMIMO performs better than small cell systems under different numbers of users at low values of θ, while the the intersect point values of θ increase with the increasing of user altitudes. Besides, we also notice that in CF-mMIMO system, aerial users can improve the coverage performance by increasing their altitudes.

To further study the impact of system parameters on the system performance, we plot Fig. 4 to show the influence of (a) BS density and (b) user altitude. With the increase of BS density, CF-mMIMO systems' coverage performance improves dramatically and approaches 1, which is attributed to the decrease in communication distance and the improvement in the power of received signal, and is explained in more detail in [12] and [32]; and an optimal density exists for the coverage performance of small cell, which is about 160 BS/km^2, due to the increase in interference. Besides, we show that an optimal altitude exists for small cell users, which is about 100 m, but such an optimal value does not exist for CF-mMIMO users, and aerial users benefit from increasing the altitudes. As previously explained, this is because BSs simultaneously serve all users, and the fact that both interference and desired signal are coming from the same BS. Therefore, for CF-mMIMO users, the ratio of the square of the summation of distances and summation of distances squared is more important (recall (46)).

Authorized licensed use limited to: Maynooth University Library. Downloaded on September 23,2025 at 15:50:34 UTC from IEEE Xplore. Restrictions apply.

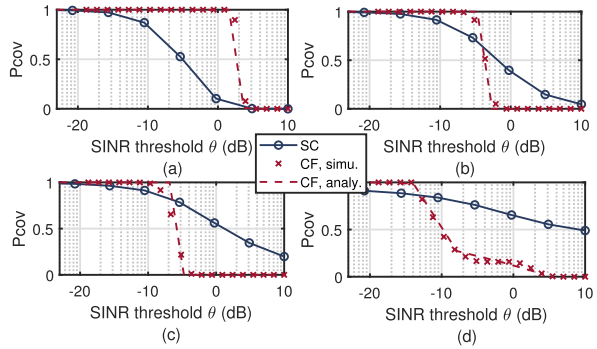

Fig. 5. Analysis and simulation results of coverage probability under $\Delta h_{au} = 100$ m, and different LoS/NLoS environments: **(a)** suburban areas, **(b)** urban areas, **(c)** dense areas, and **(d)** highrise urban areas.

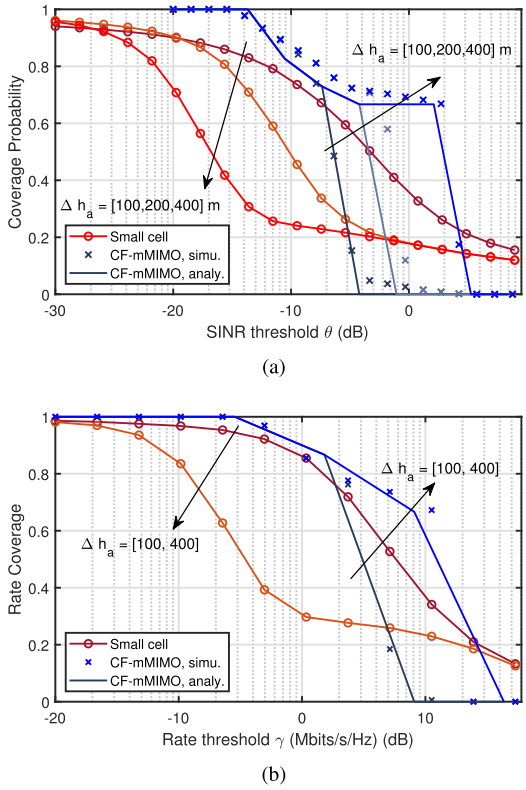

Fig. 6. Analysis and simulation results of: **(a)** coverage probability, and **(b)** rate coverage of the system, mixed of $\mathcal{N}(\mathbf{au}) = 20$ and $\mathcal{N}(\mathbf{gu}) = 10$ users under different aerial user altitudes.

Fig. 4 offers valuable insights into system design. Notably, for a fixed SINR threshold, small cell UAV users can enhance coverage probability by lowering their altitudes to approach the base stations. In contrast, CF-mMIMO UAV users can achieve improved coverage probability by increasing altitude. The maximum coverage probability for small cell UAV users, typically below 0.8 or 0.6, is markedly lower than that of CF-mMIMO UAV users, which approaches 1. Moreover, for altitudes below 200 m, CF-mMIMO consistently outperforms small cell scenarios, particularly at lower values.

Considering the influence of environment types, e.g., sub-urban areas, urban areas, etc, we plot the coverage probability under four different environments in Fig. 5. For all four different environments, the CF-mMIMO system performs better in the minimal achievable SINR compared to the small cell system. In addition, we notice that the performance of CF-mMIMO systems benefit from establishing LoS channels and it has better performance than the small cell for almost all values of θ in suburban areas, as shown in Fig. 5 (a).

Finally, we plot SINR coverage probability and rate coverage for the CF-mMIMO and small cell systems serving $\mathcal{N}(\mathbf{au}) = 20$ and $\mathcal{N}(\mathbf{gu}) = 10$ users in Fig. 6. We notice that the SINR and rate coverage performance of small cells decreases with the increase of altitude due to the increase in the serving distance, but the CF-mMIMO system benefits from increasing the aerial user altitudes. This is because in CF-mMIMO systems the ratio (between the square of the summation of the distances to all BSs and the summation of the square of distances to all BSs) matters, as seen in (46). Therefore, when the UAV altitude increases, both the power of the desired signal and the interference decreases, but their ratio increases. At the optimal altitude of small cell users ($\Delta h_{au} = 100$ m), the CF-mMIMO system performs better at low values of θ and γ ($\theta = -5$ dB and $\gamma = 3$ dB). However, if we increase the altitude of aerial users, CF-mMIMO users have better performance at larger ranges of θ and γ ($\theta = 5$ dB and $\gamma = 13$ dB).

V. Conclusion

Given that UAVs have a huge market in the next-generation networks, this work investigates the use of CF-mMIMO systems to serve a network of aerial users and ground users. Different from previous works, we use tools from stochastic geometry to model the realistic locations of randomly distributed BSs and users. Besides, we use the Nakagami-m fading model to capture the LoS/NLoS channels between BSs and users. In addition, considering that the up-tilted/down-tilted antenna model is able to improve the system performance in small cell systems, we first derive the SINR and rate coverage expressions based on the up-tilted/down-tilted antenna model and then propose the omnidirectional antenna model as a special case. To simplify the calculation, we propose an approximation that is based on computing the BS that provides the strongest signal exactly while the remaining BSs in an average sense.

Our numerical results show interesting system insights. We first show that the up-tilted/down-tilted antenna model cannot improve the SINR and rate coverage of CF-mMIMO systems due to both desired signal and interference coming from the same BSs, and multi-path fading influencing the tail SINR coverage. We show that CF-mMIMO users benefit from increasing the altitudes. While at low altitudes, CF-mMIMO users can only achieve a higher minimum achievable SINR compared to small cell users, at high altitudes, CF-mMIMO users outperform small cell users at much larger ranges of SINR and data rate.

Appendix

A. Proof of Lemma 1

By using minimum mean square error estimator, the estimated channel vector and estimation error $\hat{\mathbf{g}}_{wk}$ and $\tilde{\mathbf{g}}_{wk}$ are,

Authorized licensed use limited to: Maynooth University Library. Downloaded on September 23,2025 at 15:50:34 UTC from IEEE Xplore. Restrictions apply.

respectively, given by,

$$\hat{\mathbf{g}}_{wk} = \mathbb{E}[\mathbf{g}_{wk}\mathbf{y}_{wk}^H](\mathbb{E}[\mathbf{y}_{wk}\mathbf{y}_{wk}^H])^{-1}\mathbf{y}_{wk}, \tag{55}$$

for instance, the w-th BS is an up-tilted BS,

$$\begin{aligned}
&\mathbb{E}[\mathbf{g}_{wk}\mathbf{y}_{wk}^H] = l_{wk}^{1/2}\mathbb{E}[\mathbf{h}_{nk}(\sum_{i=1}^{\mathcal{N}(\mathbf{au})}\mathcal{G}_{au,ub}(z_{ni})\mathbf{g}_{wi}\boldsymbol{\psi}_i^H\boldsymbol{\psi}_k \\
&\quad+\sum_{j=1}^{\mathcal{N}(\mathbf{gu})}\zeta_s\mathbf{g}_{wj}\boldsymbol{\psi}_j^H\boldsymbol{\psi}_k+\frac{1}{\sqrt{\rho_p\tau_{tr}}}\mathbf{n}_{tr}\boldsymbol{\psi}_k)^H] \\
&= l_{wk}^{1/2}\mathbb{E}[\mathbf{h}_{wk}(\mathcal{G}_{au,ub}(z_{wk})\mathbf{g}_{wk}^H+\sum_{i\neq k}^{\mathcal{N}(\mathbf{au})}\mathcal{G}_{au,ub}(z_{ni})\boldsymbol{\psi}_k^H\boldsymbol{\psi}_i\mathbf{g}_{wi}^H \\
&\quad+\sum_{j=1}^{\mathcal{N}(\mathbf{gu})}\zeta_s\boldsymbol{\psi}_k^H\boldsymbol{\psi}_j\mathbf{g}_{wj}^H+\frac{1}{\sqrt{\rho_p\tau_{tr}}}\boldsymbol{\psi}_k^H\mathbf{n}_{tr}^H)] \\
&= l_{wk}^{1/2}\mathbb{E}[\mathbf{h}_{wk}\mathcal{G}_{au,ub}(z_{wk})\mathbf{g}_{wk}^H] \\
&\quad+l_{wk}^{1/2}\mathbb{E} \\
&\quad[\mathbf{h}_{wk}(\sum_{i\neq k}^{\mathcal{N}(\mathbf{au})}\mathcal{G}_{au,ub}(z_{ni})\boldsymbol{\psi}_k^H\boldsymbol{\psi}_i\mathbf{g}_{wi}^H+\sum_{j=1}^{\mathcal{N}(\mathbf{gu})}\zeta_s\boldsymbol{\psi}_k^H\boldsymbol{\psi}_j\mathbf{g}_{wj}^H)] \\
&= l_{wk}\mathcal{G}_{au,ub}(z_{wk})\mathbb{E}[\mathbf{h}_{wk}\mathbf{h}_{wk}^H] = l_{wk}\mathcal{G}_{au,ub}(z_{wk})\mathbf{I}_{N_a},
\end{aligned}$$

$$\begin{aligned}
&\mathbb{E}[\mathbf{y}_{wk}\mathbf{y}_{wk}^H] = \mathbb{E}[(\mathcal{G}_{au,ub}(z_{wk})\mathbf{g}_{wk}+\sum_{i\neq k}^{\mathcal{N}(\mathbf{au})}\mathcal{G}_{au,ub}(z_{wi}) \\
&\quad\times\mathbf{g}_{wi}\boldsymbol{\psi}_i^H\boldsymbol{\psi}_k+\sum_{j=1}^{\mathcal{N}(\mathbf{gu})}\zeta_s\mathbf{g}_{wj}\boldsymbol{\psi}_j^H\boldsymbol{\psi}_k+\frac{1}{\sqrt{\rho_p\tau_{tr}}}\mathbf{n}_{tr}\boldsymbol{\psi}_k) \\
&(\mathcal{G}_{au,ub}(z_{wk})\mathbf{g}_{wk}+\sum_{i\neq k}^{\mathcal{N}(\mathbf{au})}\mathcal{G}_{au,ub}(z_{wi})\mathbf{g}_{wi}\boldsymbol{\psi}_i^H\boldsymbol{\psi}_k \\
&\quad+\sum_{j=1}^{\mathcal{N}(\mathbf{gu})}\zeta_s\mathbf{g}_{wj}\boldsymbol{\psi}_j^H\boldsymbol{\psi}_k+\frac{1}{\sqrt{\rho_p\tau_{tr}}}\mathbf{n}_{tr}\boldsymbol{\psi}_k)^H] \\
&= \mathcal{G}_{au,ub}^2(z_{wk})\mathbb{E}[\mathbf{g}_{wk}\mathbf{g}_{wk}^H]+\mathbb{E}[\sum_{i\neq k}^{\mathcal{N}(\mathbf{au})}\mathcal{G}_{au,ub}(z_{wi})\boldsymbol{\psi}_k^H\boldsymbol{\psi}_i\mathbf{g}_{wi}^H \\
&\quad\times(\sum_{i\neq k}^{\mathcal{N}(\mathbf{au})}\mathcal{G}_{au,ub}(z_{wi})\boldsymbol{\psi}_k^H\boldsymbol{\psi}_i\mathbf{g}_{wi}^H)]+\mathbb{E}[\sum_{j=1}^{\mathcal{N}(\mathbf{gu})}\zeta_s\mathbf{g}_{wj}\boldsymbol{\psi}_j^H\boldsymbol{\psi}_k \\
&\quad\times(\sum_{j=1}^{\mathcal{N}(\mathbf{gu})}\zeta_s\boldsymbol{\psi}_k^H\boldsymbol{\psi}_j\mathbf{g}_{wj}^H)]+\frac{1}{\rho_p\tau_{tr}}\mathbb{E}[\mathbf{n}_{tr}\boldsymbol{\psi}_k\boldsymbol{\psi}_k^H\mathbf{n}_{tr}^H] \\
&= \sum_{i=1}^{\mathcal{N}(\mathbf{au})}l_{wi}\mathcal{G}_{au,ub}^2(z_{wi})|\boldsymbol{\psi}_i^H\boldsymbol{\psi}_k|^2\mathbf{I}_{N_a} \\
&\quad+\sum_{j=1}^{\mathcal{N}(\mathbf{gu})}l_{wj}\mathcal{G}_{gu,ub}^2(z_{wj})|\boldsymbol{\psi}_j^H\boldsymbol{\psi}_k|^2\mathbf{I}_{N_a}+\frac{1}{\rho_p\tau_{tr}}\mathbf{I}_{N_a},
\end{aligned} \tag{56}$$

the down-tilted BS follows a similar way, and the proof completes by simplifying the above equations and let $\beta_{wk} = \frac{\mathcal{G}_{v,b}(z_{wk})l_{wk}}{\sum_{i=1}^{K}l_{wi}\mathcal{G}_{v,b}^2(z_{wi})|\boldsymbol{\psi}_i^H\boldsymbol{\psi}_k|^2+\frac{1}{\rho_p\tau_{tr}}}$.

B. Proof of Lemma 2

The $\mathbb{E}[|T_0|^2]$, $\mathbb{E}[|T_1|^2]$, $\mathbb{E}[|T_2|^2]$, and $\mathbb{E}[|T_3|^2]$ are computed as follows,

$$\begin{aligned}
&\mathbb{E}[|T_0|^2] = \rho_b\Big(\sum_{w=1}^{\mathcal{N}(b_{ub})}\sqrt{\eta_{wo}}\mathcal{G}_{o,ub}(z_{wo})\mathbb{E}[\hat{\mathbf{g}}_{wo}^T\hat{\mathbf{g}}_{wo}^*]s_o \\
&\quad+\sum_{w=1}^{\mathcal{N}(b_{db})}\sqrt{\eta_{wk}}\mathcal{G}_{o,db}(z_{wo})\mathbb{E}[\hat{\mathbf{g}}_{wo}^T\hat{\mathbf{g}}_{wo}^*]s_o\Big)^2 \\
&= \rho_b N_a^2\Big(\sum_{w=1}^{N_{bs}}\sqrt{\eta_{wo}}\mathcal{G}_{o,b}^2(z_{wo})l_{wo}\beta_{wo}\Big)^2, \\
&\mathbb{E}[|T_1|^2] \\
&= \mathbb{E}[|\sum_{w=1}^{N_{bs}}\sqrt{\rho_b\eta_{wo}}\mathcal{G}_{o,b}(z_{wo})(\hat{\mathbf{g}}_{wo}^T\hat{\mathbf{g}}_{wo}^*-\mathbb{E}[\hat{\mathbf{g}}_{wo}^T\hat{\mathbf{g}}_{wo}^*])s_o|^2] \\
&= \sum_{w=1}^{N_{bs}}\rho_b\eta_{wo}\mathcal{G}_{o,b}^2(z_{wo})(\mathbb{E}[|\hat{\mathbf{g}}_{wo}^T\hat{\mathbf{g}}_{wo}^*|^2]-\mathbb{E}^2[\hat{\mathbf{g}}_{wo}^T\hat{\mathbf{g}}_{wo}^*]) \\
&= \sum_{w=1}^{N_{bs}}\rho_b\eta_{wo}\mathcal{G}_{o,b}^2(z_{wo})N_a^2\Big(\mathcal{G}_{o,b}^2(r_{wo})l_{wo}^2\beta_{wo}^2 \\
&\quad+\beta_{wo}^4\sum_{i=1}^{K}|\boldsymbol{\psi}_i^H\boldsymbol{\psi}_o|^4\mathcal{G}_{v,b}^4(z_{wi})l_{wi}^2\Big(\frac{1}{m_c}-1\Big)\Big), \\
&\mathbb{E}[|T_2|^2] = \mathbb{E}[|\sum_{w=1}^{N_{bs}}\sum_{i\neq o}^{K}\sqrt{\rho_b\eta_{wi}}\mathcal{G}_{o,b}(z_{wo})\hat{\mathbf{g}}_{wo}^T\hat{\mathbf{g}}_{wi}^*s_i|^2] \\
&= \sum_{w=1}^{N_{bs}}\sum_{i\neq o}^{K}\rho_b\eta_{wi}\mathcal{G}_{o,b}^2(z_{wo})\mathbb{E}[|\hat{\mathbf{g}}_{wo}^T\hat{\mathbf{g}}_{wi}^*|^2] \\
&= N_a^2\sum_{w=1}^{N_{bs}}\sum_{i\neq o}^{K}\rho_b\eta_{wi}\mathcal{G}_{o,b}^3(z_{wo})\mathcal{G}_{v,b}(z_{wi})l_{wo}\beta_{wi}l_{wi}\beta_{wi}, \\
&\mathbb{E}[|T_3|^2] = \mathbb{E}[|\sum_{w=1}^{N_{bs}}\sum_{i=1}^{K}\sqrt{\rho_b\eta_{wi}}\mathcal{G}_{o,b}(z_{wo})\tilde{\mathbf{g}}_{wo}^T\hat{\mathbf{g}}_{wi}^*s_i|^2] \\
&= \sum_{w=1}^{N_{bs}}\sum_{i=1}^{K}\rho_b\eta_{wi}\mathcal{G}_{o,b}^2(z_{wo})\mathbb{E}[\tilde{\mathbf{g}}_{wo}^T\tilde{\mathbf{g}}_{wo}^*\tilde{\mathbf{g}}_{wo}^T\hat{\mathbf{g}}_{wi}^*] \\
&= N_a^2\sum_{w=1}^{N_{bs}}\sum_{i=1}^{K}\rho_b\eta_{wi}\mathcal{G}_{o,b}^3(z_{wo})\mathcal{G}_{v,b}(z_{wi})\Big(l_{wo}-l_{wo}\beta_{wo}\Big)l_{wi}\beta_{wi}.
\end{aligned} \tag{57}$$

Substituting the above values, we obtain the results presented in Lemma 2.

C. Proof of Lemma 3

In the case of $p_{los,1}$, it means that the strongest signal is from the BSs, either w_{db} or w_{ub}, providing a side-lobe to the typical user. Therefore, the signal from BSs that provides main-lobe should be at least d_l away: $r^{-\alpha_l} > \zeta_m^3 d_l^{-\alpha_l}$, which implies that $d_l > \zeta_m^{\frac{3}{\alpha_l}} r$. The $\min(\cdot,\cdot)$ and $\max(\cdot,\cdot)$ in (26) are used to constraint the range of the locations. Consequently, the probability of $p_{los,1}$ is obtained by the multiplication of the PDF of the side-lobe BS is located at z ($z < z_{g,1}$)

Authorized licensed use limited to: Maynooth University Library. Downloaded on September 23,2025 at 15:50:34 UTC from IEEE Xplore. Restrictions apply.

and the main-lobe BS is located further than $d_l(r)$. The other scenarios follow the same method.

D. Proof of Lemma 4

Let $N_{bs,l}$ and $N_{bs,n}$ be the number of BSs, including b_{db} and b_{ub}, that established LoS and NLoS channels with the typical user. The signal term is given by

$$\begin{aligned}\mathrm{S} &= \sum_{w=1}^{N_{bs}} \sqrt{\mathcal{G}_{o,b}^3(z_{wo}) l_{wo}\beta_{wo}} \\ &= \sum_{w_l=1}^{N_{bl}} \sqrt{\mathcal{G}_{o,b}^3(z_{w_lo}) l_{w_lo}\beta_{w_lo}} + \sum_{w_n=1}^{N_{bn}} \sqrt{\mathcal{G}_{o,b}^3(z_{w_no}) l_{w_no}\beta_{w_no}} \\ &= \mathrm{S}_l(r_l) + \mathrm{S}_n(r_n). \end{aligned} \tag{58}$$

In the case that the strongest LoS BS is located within $B(0, z_{g,1})$ ($p_{los,1}$) at distance r away from the typical user, the nearest LoS BS that establish main-lobe with the typical user is located at least at distance d_l away. To simplify the notations, we assume that BSs are ordered. That is, the LoS BS with the strongest signal is denoted by $w_l = 1$ in the summation in (59). Hence, the $\mathrm{S}_{l,1}(r_l)$ is approximated as

$$\begin{aligned}&\sum_{w_l=1}^{N_{bs,l}} \sqrt{\mathcal{G}_{o,b}^3(r_{w_lo}) l_{w_lo}\beta_{w_lo}} = \sqrt{\mathcal{G}_{o,b}^3(r_{1o}) l_{1o}\beta_{1o}} \\ &\quad + \sum_{w_l=2}^{N_{bs,l}} \sqrt{\mathcal{G}_{o,b}^3(r_{w_lo}) l_{w_lo}\beta_{w_lo}} \\ &\approx \sqrt{\mathcal{G}_{o,b}^3(r_{1o}) l_{1o}\beta_{1o}} + \mathbb{E}\Bigg[\sum_{w_l=2}^{N_{bs,l}} \sqrt{\mathcal{G}_{o,b}^3(r_{w_lo}) l_{w_lo}\beta_{w_lo}}\Bigg] \\ &\overset{(a)}{=} l_{1o}\beta_{1o} + \mathbb{E}\Bigg[\sum_{b\in B(r_{lo},z_{g,1})} \sqrt{l_{bo}\beta_{bo}}\Bigg] \\ &\quad + \mathbb{E}\Bigg[\sum_{b_g\in B(d_l,z_{g,2})} \sqrt{\zeta_m^3 l_{b_go}\beta_{b_go}}\Bigg] \\ &\quad + \mathbb{E}\Bigg[\sum_{b_{db}\in B(z_{g,1},z_{g,2})} \sqrt{l_{b_{db}o}\beta_{b_{db}o}}\Bigg] v + \mathbb{E}\Bigg[\sum_{b\in B(z_{g,2},\infty)} \sqrt{l_{bo}\beta_{bo}}\Bigg], \end{aligned} \tag{59}$$

in which the step (a) follows that the strongest BS is located within $B(0, z_{g,1})$, thus, the user experience a side-lobe gain, the first expectation term is the mean of the siganl of remaining BSs within $B(0, z_{g,1})$, the second expectation term is the mean of the signal from the BS that provides the main-lobe gain to the typical user, which should be located at least d_l away, similarly, the third and the fourth expectation terms are the mean of the signal from the remaining BSs,

$$\begin{aligned}&\mathbb{E}\Bigg[\sum_{b\in B(r_{lo},z_{g,1})} \sqrt{l_{bo}\beta_{bo}}\Bigg] \\ &\overset{(b)}{=} 2\pi\lambda_b \int_{r_{lo}}^{z_{g,1}} \frac{P_l(r) r^{-\alpha_l}}{\sqrt{r^{-\alpha_{\{l,n\}}} + \frac{1}{\rho_p\tau_{tr}}}} \mathrm{d}r, \end{aligned} \tag{60}$$

in which step (b) follows Campbell's theorem [55] with conversion from Cartesian to polar coordinates, and the density of LoS BSs within $B(r_{lo}, z_{g,1})$ is $\lambda_b P_l(r)$. The other expectation terms, as well as $\mathrm{S}_n(r_n)$ and the interference term, follows a similar way, thus, omitted here.

E. Proof of Corollary 2

Similar to previous proof, BSs are divided into LoS and NLoS, and $w = 1$ denotes the nearest LoS or NLoS BS. The numerator is approximated as

$$\begin{aligned}&\Bigg(\sum_{w=1}^{N_{bs}} \sqrt{l_{wo}\beta_{wo}}\Bigg)^2 \approx \Bigg(\sqrt{l_{1o,l}\beta_{1o,l}} \\ &\quad + \mathbb{E}[\sum_{w=2}^{N_{bs,l}} \sqrt{l_{wo,l}\beta_{wo,l}} \mid l_{1o,l}] \\ &\quad + \sqrt{l_{1o,n}\beta_{1o,n}} + \mathbb{E}[\sum_{w=2}^{N_{bs,n}} \sqrt{l_{wo,n}\beta_{wo,n}} \mid l_{1o,n}]\Bigg)^2 \\ &= \Bigg(\frac{r_{1o,l}^{-\alpha_l}}{\sqrt{r_{1o,l}^{-\alpha_l} + \frac{1}{\rho_p\tau_{tr}}}} + \frac{r_{1o,n}^{-\alpha_n}}{\sqrt{r_{1o,n}^{-\alpha_n} + \frac{1}{\rho_p\tau_{tr}}}} + 2\pi\lambda_b(\kappa_l(r_{1o,l}) \\ &\quad + \kappa_l(r_{1o,n}))\Bigg)^2, \end{aligned} \tag{61}$$

and the denominator is approximated as

$$\begin{aligned}&K\sum_{w=1}^{N_{bs}} l_{wo} + \sum_{w=1}^{N_{bs}} \beta_{wo}^3 l_{wo}(\frac{1}{m_l} - 1) \\ &\approx K(l_{1o,l} + l_{1o,n}) + \beta_{1o,l}^3 l_{1o,l}(\frac{1}{m_c} - 1) + \mathbb{E}\Bigg[\sum_{w=2}^{N_{bs,l}} \Bigg(K l_{wo,l} \\ &\quad + \beta_{wo,l}^3 l_{wo}(\frac{1}{m_l} - 1)\Bigg) \mid l_{1o,l}\Bigg] + \mathbb{E}\Bigg[\sum_{w=2}^{N_{bs,n}} K l_{wo,n} \mid l_{1o,n}\Bigg] \\ &= K(r_{1o,l}^{-\alpha_l} + r_{1o,n}^{-\alpha_n}) + \frac{r_{1o,l}^{-4\alpha_l}(\frac{1}{m_l} - 1)}{(r_{1o,l}^{-\alpha_l} + \frac{1}{\rho_p\tau_{tr}})^3} + \kappa_1(r_{1o,l}) \\ &\quad + \kappa_2(r_{1o,n}). \end{aligned} \tag{62}$$

REFERENCES

[1] J. F. Campbell, D. C. Sweeney, and J. Zhang, "Strategic design for delivery with trucks and drones," *Proc. Supply Chain Anal. Rep. SCMA*, pp. 47–55, Apr. 2017.

[2] Y. Qin, M. A. Kishk, and M.-S. Alouini, "Energy efficiency analysis of charging pads-powered UAV-enabled wireless networks," *IEEE Trans. Wireless Commun.*, vol. 22, no. 7, pp. 4683–4697, Jul. 2023.

[3] H. Shakhatreh et al., "Unmanned aerial vehicles (UAVs): A survey on civil applications and key research challenges," *IEEE Access*, vol. 7, pp. 48572–48634, 2019.

[4] M. Alzenad and H. Yanikomeroglu, "Coverage and rate analysis for vertical heterogeneous networks (VHetNets)," *IEEE Trans. Wireless Commun.*, vol. 18, no. 12, pp. 5643–5657, Dec. 2019.

[5] Y. Qin, M. A. Kishk, and M.-S. Alouini, "Performance evaluation of UAV-enabled cellular networks with battery-limited drones," *IEEE Commun. Lett.*, vol. 24, no. 12, pp. 2664–2668, Dec. 2020.

[6] M. Matracia, M. A. Kishk, and M.-S. Alouini, "Coverage analysis for UAV-assisted cellular networks in rural areas," *IEEE Open J. Veh. Technol.*, vol. 2, pp. 194–206, 2021.

[7] Y. Qin, M. A. Kishk, and M.-S. Alouini, "Drone charging stations deployment in rural areas for better wireless coverage: Challenges and solutions," *IEEE Internet Things Mag.*, vol. 5, no. 1, pp. 148–153, Mar. 2022.

Authorized licensed use limited to: Maynooth University Library. Downloaded on September 23,2025 at 15:50:34 UTC from IEEE Xplore. Restrictions apply.

[8] M. Khosravi, S. Enayati, H. Saeedi, and H. Pishro-Nik, "Multi-purpose drones for coverage and transport applications," *IEEE Trans. Wireless Commun.*, vol. 20, no. 6, pp. 3974–3987, Jun. 2021.

[9] Y. Qin, M. A. Kishk, and M.-S. Alouini, "Stochastic-geometry-based analysis of multipurpose UAVs for package and data delivery," *IEEE Internet Things J.*, vol. 10, no. 5, pp. 4664–4676, Mar. 2023.

[10] S. Chen, J. Zhang, J. Zhang, E. Björnson, and B. Ai, "A survey on user-centric cell-free massive MIMO systems," *Digit. Commun. Netw.*, vol. 8, no. 5, pp. 695–719, Oct. 2022.

[11] C. D'Andrea, A. Garcia-Rodriguez, G. Geraci, L. G. Giordano, and S. Buzzi, "Analysis of UAV communications in cell-free massive MIMO systems," *IEEE Open J. Commun. Soc.*, vol. 1, pp. 133–147, 2020.

[12] H. Q. Ngo, A. Ashikhmin, H. Yang, E. G. Larsson, and T. L. Marzetta, "Cell-free massive MIMO versus small cells," *IEEE Trans. Wireless Commun.*, vol. 16, no. 3, pp. 1834–1850, Mar. 2017.

[13] L. Chen, M. A. Kishk, and M.-S. Alouini, "Dedicating cellular infrastructure for aerial users: Advantages and potential impact on ground users," *IEEE Trans. Wireless Commun.*, vol. 22, no. 4, pp. 2523–2535, Apr. 2023.

[14] S. Chandrasekharan et al., "Designing and implementing future aerial communication networks," *IEEE Commun. Mag.*, vol. 54, no. 5, pp. 26–34, May 2016.

[15] Y. Zeng, J. Lyu, and R. Zhang, "Cellular-connected UAV: Potential, challenges, and promising technologies," *IEEE Wireless Commun.*, vol. 26, no. 1, pp. 120–127, Feb. 2019.

[16] Y. Qin, M. A. Kishk, and M.-S. Alouini, "Coverage analysis and trajectory optimization for aerial users with dedicated cellular infrastructure," *IEEE Trans. Wireless Commun.*, vol. 23, no. 4, pp. 3042–3056, Apr. 2024.

[17] H. C. Nguyen, R. Amorim, J. Wigard, I. Z. Kovács, T. B. Sørensen, and P. E. Mogensen, "How to ensure reliable connectivity for aerial vehicles over cellular networks," *IEEE Access*, vol. 6, pp. 12304–12317, 2018.

[18] M. M. Azari, F. Rosas, K.-C. Chen, and S. Pollin, "Ultra reliable UAV communication using altitude and cooperation diversity," *IEEE Trans. Commun.*, vol. 66, no. 1, pp. 330–344, Jan. 2018.

[19] M. M. Azari, F. Rosas, K.-C. Chen, and S. Pollin, "Optimal UAV positioning for terrestrial-aerial communication in presence of fading," in *Proc. IEEE Global Commun. Conf. (GLOBECOM)*, Dec. 2016, pp. 1–7.

[20] Y. Zeng and R. Zhang, "Energy-efficient UAV communication with trajectory optimization," *IEEE Trans. Wireless Commun.*, vol. 16, no. 6, pp. 3747–3760, Jun. 2017.

[21] S. Zhang, H. Zhang, Q. He, K. Bian, and L. Song, "Joint trajectory and power optimization for UAV relay networks," *IEEE Commun. Lett.*, vol. 22, no. 1, pp. 161–164, Jan. 2018.

[22] G. Geraci, A. Garcia-Rodriguez, L. Galati Giordano, D. López-Pérez, and E. Björnson, "Understanding UAV cellular communications: From existing networks to massive MIMO," *IEEE Access*, vol. 6, pp. 67853–67865, 2018.

[23] Y. Li, A. H. Aghvami, and D. Dong, "Path planning for cellular-connected UAV: A DRL solution with quantum-inspired experience replay," *IEEE Trans. Wireless Commun.*, vol. 21, no. 10, pp. 7897–7912, Oct. 2022.

[24] X. Pang et al., "Uplink precoding optimization for NOMA cellular-connected UAV networks," *IEEE Trans. Commun.*, vol. 68, no. 2, pp. 1271–1283, Feb. 2020.

[25] Q. Fu and J. Liu, "Generalized multi-hop NR sidelink relay for future V2X communication," *IEEE/ACM Trans. Netw.*, vol. 32, no. 2, pp. 1691–1706, Apr. 2024.

[26] Q. Fu, J. Liu, and J. Wang, "A flexible resource allocation scheme for NR V2X based vulnerable road user protection," *IEEE Trans. Veh. Technol.*, vol. 73, no. 5, pp. 6672–6686, May 2024.

[27] K. Xiong, Z. Wang, S. Leng, and J. He, "A digital-twin-empowered lightweight model-sharing scheme for multirobot systems," *IEEE Internet Things J.*, vol. 10, no. 19, pp. 17231–17242, Oct. 2023.

[28] H. Guo, Y. Wang, J. Liu, and C. Liu, "Multi-UAV cooperative task offloading and resource allocation in 5G advanced and beyond," *IEEE Trans. Wireless Commun.*, vol. 23, no. 1, pp. 347–359, Jan. 2024.

[29] K. Xiong, R. Wang, S. Leng, C. Huang, and C. Yuen, "RIS-empowered topology control for decentralized federated learning in urban air mobility," *IEEE Internet Things J.*, early access, Sep. 6, 2024, doi: 10.1109/JIOT.2024.3453964.

[30] S. Elhoushy, M. Ibrahim, and W. Hamouda, "Cell-free massive MIMO: A survey," *IEEE Commun. Surveys Tuts.*, vol. 24, no. 1, pp. 492–523, 1st Quart., 2022.

[31] H. Q. Ngo, G. Interdonato, E. G. Larsson, G. Caire, and J. G. Andrews, "Ultradense cell-free massive MIMO for 6G: Technical overview and open questions," *Proc. IEEE*, vol. 112, no. 7, pp. 805–831, Jul. 2024.

[32] H. Q. Ngo, A. Ashikhmin, H. Yang, E. G. Larsson, and T. L. Marzetta, "Cell-free massive MIMO: Uniformly great service for everyone," in *Proc. IEEE 16th Int. Workshop Signal Process. Adv. Wireless Commun. (SPAWC)*, Jun. 2015, pp. 201–205.

[33] J. Zhang, S. Chen, Y. Lin, J. Zheng, B. Ai, and L. Hanzo, "Cell-free massive MIMO: A new next-generation paradigm," *IEEE Access*, vol. 7, pp. 99878–99888, 2019.

[34] E. Björnson and L. Sanguinetti, "Scalable cell-free massive MIMO systems," *IEEE Trans. Commun.*, vol. 68, no. 7, pp. 4247–4261, Jul. 2020.

[35] S. Chen, J. Zhang, E. Björnson, J. Zhang, and B. Ai, "Structured massive access for scalable cell-free massive MIMO systems," *IEEE J. Sel. Areas Commun.*, vol. 39, no. 4, pp. 1086–1100, Apr. 2021.

[36] G. Interdonato, M. Karlsson, E. Bjornson, and E. G. Larsson, "Downlink spectral efficiency of cell-free massive MIMO with full-pilot zero-forcing," in *Proc. IEEE Global Conf. Signal Inf. Process. (GlobalSIP)*, Nov. 2018, pp. 1003–1007.

[37] G. Interdonato, M. Karlsson, E. Björnson, and E. G. Larsson, "Local partial zero-forcing precoding for cell-free massive MIMO," *IEEE Trans. Wireless Commun.*, vol. 19, no. 7, pp. 4758–4774, Jul. 2020.

[38] Y. Zhao, I. G. Niemegeers, and S. H. De Groot, "Power allocation in cell-free massive MIMO: A deep learning method," *IEEE Access*, vol. 8, pp. 87185–87200, 2020.

[39] J. Zhang, Y. Wei, E. Björnson, Y. Han, and S. Jin, "Performance analysis and power control of cell-free massive MIMO systems with hardware impairments," *IEEE Access*, vol. 6, pp. 55302–55314, 2018.

[40] H. Masoumi and M. J. Emadi, "Performance analysis of cell-free massive MIMO system with limited fronthaul capacity and hardware impairments," *IEEE Trans. Wireless Commun.*, vol. 19, no. 2, pp. 1038–1053, Feb. 2019.

[41] J. Zheng, J. Zhang, L. Zhang, X. Zhang, and B. Ai, "Efficient receiver design for uplink cell-free massive MIMO with hardware impairments," *IEEE Trans. Veh. Technol.*, vol. 69, no. 4, pp. 4537–4541, Apr. 2020.

[42] S. Buzzi and C. D'Andrea, "Cell-free massive MIMO: User-centric approach," *IEEE Wireless Commun. Lett.*, vol. 6, no. 6, pp. 706–709, Dec. 2017.

[43] Y. Zhang, W. Xia, H. Zhao, G. Zheng, S. Lambotharan, and L. Yang, "Performance analysis of RIS-assisted cell-free massive MIMO systems with transceiver hardware impairments," *IEEE Trans. Commun.*, vol. 71, no. 12, pp. 7258–7272, Dec. 2023.

[44] A. Papazafeiropoulos, P. Kourtessis, M. Di Renzo, S. Chatzinotas, and J. M. Senior, "Performance analysis of cell-free massive MIMO systems: A stochastic geometry approach," *IEEE Trans. Veh. Technol.*, vol. 69, no. 4, pp. 3523–3537, Apr. 2020.

[45] Z. Chen and E. Björnson, "Channel hardening and favorable propagation in cell-free massive MIMO with stochastic geometry," *IEEE Trans. Commun.*, vol. 66, no. 11, pp. 5205–5219, Nov. 2018.

[46] P. Parida and H. S. Dhillon, "Cell-free massive MIMO with finite fronthaul capacity: A stochastic geometry perspective," *IEEE Trans. Wireless Commun.*, vol. 22, no. 3, pp. 1555–1572, Mar. 2023.

[47] S. Kusaladharma, W.-P. Zhu, W. Ajib, and G. A. A. Baduge, "Stochastic geometry based performance characterization of SWIPT in cell-free massive MIMO," *IEEE Trans. Veh. Technol.*, vol. 69, no. 11, pp. 13357–13370, Nov. 2020.

[48] S. Elhoushy and W. Hamouda, "Limiting Doppler shift effect on cell-free massive MIMO systems: A stochastic geometry approach," *IEEE Trans. Wireless Commun.*, vol. 20, no. 9, pp. 5656–5671, Sep. 2021.

[49] M. Ibrahim, S. Elhoushy, and W. Hamouda, "Uplink performance of MmWave-fronthaul cell-free massive MIMO systems," *IEEE Trans. Veh. Technol.*, vol. 71, no. 2, pp. 1536–1548, Feb. 2021.

[50] X. Ma, X. Lei, X. Zhou, and X. Tang, "Secrecy performance evaluation of scalable cell-free massive MIMO systems: A stochastic geometry approach," *IEEE Trans. Inf. Forensics Secur.*, vol. 18, pp. 2826–2841, 2023.

[51] S. Mukherjee and J. Lee, "Edge computing-enabled cell-free massive MIMO systems," *IEEE Trans. Wireless Commun.*, vol. 19, no. 4, pp. 2884–2899, Apr. 2020.

[52] A. Al-Hourani, S. Kandeepan, and S. Lardner, "Optimal LAP altitude for maximum coverage," *IEEE Wireless Commun. Lett.*, vol. 3, no. 6, pp. 569–572, Dec. 2014.

Authorized licensed use limited to: Maynooth University Library. Downloaded on September 23,2025 at 15:50:34 UTC from IEEE Xplore. Restrictions apply.

[53] Y. Qin, M. A. Kishk, and M.-S. Alouini, "A dominant interferer plus mean field-based approximation for SINR meta distribution in wireless networks," *IEEE Trans. Commun.*, vol. 71, no. 6, pp. 3663–3678, Jun. 2023.

[54] H. K. Armeniakos, A. G. Kanatas, and H. S. Dhillon, "Comprehensive analysis of maximum power association policy for cellular networks using distance and angular coordinates," *IEEE Trans. Wireless Commun.*, vol. 23, no. 9, pp. 12189–12205, Sep. 2024.

[55] M. Haenggi, *Stochastic Geometry for Wireless Networks*. Cambridge, U.K.: Cambridge Univ. Press, 2012.

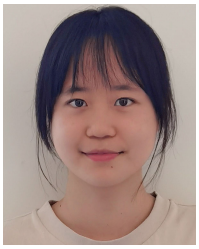

Yujie Qin (Member, IEEE) received the B.Sc. degree from the University of Electronic Science and Technology of China (UESTC) in 2020 and the M.Sc. degree from King Abdullah University of Science and Technology (KAUST) in 2021, where she is currently pursuing the Ph.D. degree with the Communication Theory Laboratory. Her current research interests include stochastic geometry and UAV communication.

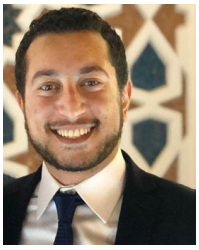

Mustafa A. Kishk (Member, IEEE) received the B.Sc. and M.Sc. degrees in electrical engineering from Cairo University, Giza, Egypt, in 2013 and 2015, respectively, and the Ph.D. degree in electrical engineering from Virginia Tech, Blacksburg, VA, USA, in 2018. He is currently an Assistant Professor with the Electronic Engineering Department, Maynooth University, Ireland. Before that, he was a Post-Doctoral Research Fellow with the Communication Theory Laboratory, King Abdullah University of Science and Technology, Saudi Arabia. His current research interests include stochastic geometry, UAV-enabled communication systems, and satellite-enabled communications. He was a recipient of the IEEE ComSoc Outstanding Young Researcher Award for Europe, Middle East, and Africa Region in 2022. He was recognized as an Exemplary Reviewer by the IEEE COMMUNICATIONS LETTERS in 2020. He currently serves as an Associate Editor for IEEE WIRELESS COMMUNICATION LETTERS.

Mohamed-Slim Alouini (Fellow, IEEE) was born in Tunis, Tunisia. He received the Ph.D. degree in electrical engineering from California Institute of Technology (Caltech), Pasadena, CA, USA, in 1998. He was a Faculty Member of the University of Minnesota, Minneapolis, MN, USA, and then Texas A&M University at Qatar, Education City, Doha, Qatar, before joining King Abdullah University of Science and Technology (KAUST), Thuwal, Makkah, Saudi Arabia, as a Professor in electrical engineering in 2009. His current research interests include the modeling, design, and performance analysis of wireless communication systems.

Authorized licensed use limited to: Maynooth University Library. Downloaded on September 23,2025 at 15:50:34 UTC from IEEE Xplore. Restrictions apply.